Bering Sea surface water conditions during Marine Isotope Stages 12 to 10 at Navarin Canyon (IODP Site U1345)

Beth E. Caissie[1], Julie Brigham-Grette[2], Mea S. Cook[3], Elena Colmenero-Hidalgo[4]

[1]{Iowa State University, Ames, Iowa}

[2]{University of Massachusetts, Amherst, Amherst, Massachusetts}

[3]{Williams College, Williamstown, Massachusetts}

[4]{Universidad de León, León, Spain}

Correspondence to: B.E. Caissie (bethc@iastate.edu)

Abstract

Records of past warm periods are essential for understanding interglacial climate system dynamics. Marine Isotope Stage 11 occurred 425-394 ka when global ice volume was the lowest, sea level was the highest and terrestrial temperatures were the warmest of the last 500 kyrs. Because of its extreme character, this interval has been considered an analog for the next century of climate change. The Bering Sea is ideally situated to record how opening or closing of the Pacific-Arctic Ocean gateway (Bering Strait) impacted primary productivity, sea ice, and sediment transport in the past; however, little is known about this region prior to 125 ka. IODP Expedition 323 to the Bering Sea offered the unparalleled opportunity to look in detail at time periods older than had been previously retrieved using gravity and piston cores. Here we present a multi-proxy record for Marine Isotope Stages 12-10 from Site U1345 located near the continental shelf-slope break. MIS 11 is bracketed by highly productive laminated intervals that may have been triggered by flooding of the Beringian shelf. Although sea ice is reduced during the early MIS 11 laminations, it remains present at the site throughout both glacials and MIS 11.

High summer insolation is associated with higher productivity, but colder SSTs, which implies that productivity was likely driven by increased upwelling. Multiple examples of Pacific-Atlantic teleconnections are presented including laminations deposited at the end of MIS 11 in synchrony with millennial-scale expansions in sea ice in the Bering Sea and stadial events seen in the North Atlantic. When global eustatic sea level was at its peak, a series of anomalous conditions are seen at U1345. We examine whether this is evidence for a reversal of Bering Strait Through Flow, an advance of Beringian tidewater glaciers, or a turbidite.

1 Introduction

Predictions and modeling of future climate change require a detailed understanding of how the climate system works. Reconstructions of previous warm intervals shed light on interhemispheric teleconnections. The most recent interglacial period with orbital conditions similar to today was approximately 400 ka, during the extremely long interglacial known as Marine Isotope Stage (MIS) 11. CO_2 concentration averaged approximately 275 ppm, which is similar to pre-industrial levels (EPICA Community Members, 2004). The transition from MIS 12 into MIS 11 has been compared to the last deglaciation (Dickson et al., 2009) and extreme warmth during MIS 11 has been considered an analog for future warmth (Droxler et al., 2003; Loutre and Berger, 2003), although the natural course of interglacial warmth today has been disrupted by anthropogenic forcing (IPCC, 2013).

Despite the work done to characterize the warmth of MIS 11 in the terrestrial realm (Candy et al., 2014; Melles et al., 2012; Prokopenko et al., 2010), as well as the North Atlantic (Bauch et al., 2000; Chaisson et al., 2002; Dickson et al., 2009; Milker et al., 2013; Poli et al., 2010), little is known about this interval from the North Pacific and Bering Sea region (Candy et al., 2014). Modeling studies describe several mechanisms for linking the Atlantic and Pacific through oceanic heat transport on glacial-interglacial time scales (DeBoer and Nof, 2004; Hu et al., 2010), however, there have been no tests of these modeling studies using proxy data older than 30 ka. Furthermore, the location of the Bering Sea marginal sea ice zone advanced and retreated hundreds of kilometers during

the past three glacial-interglacial cycles (Caissie et al., 2010; Katsuki and Takahashi, 2005; Sancetta and Robinson, 1983); however, sea surface and intermediate water variability before MIS 5 is unknown.

This investigation of terrestrial-marine coupling at the shelf-slope break from MIS 12 to 10 is the first study of this interval in the subarctic Pacific (Fig. 1). We use a multi-proxy approach to examine orbital- and millennial-scale changes in productivity and sea ice extent. We demonstrate that insolation plays a major role in these changes, but that sea ice also shows rapid, millennial-scale variability. Finally, we test the hypotheses that 1) in Beringia, tidewater glaciers advanced while sea level was high and 2) Bering Strait Through Flow reversed shortly after the MIS 12 glacial termination (Termination V). We find inconclusive evidence of a glacial advance, but no evidence of Bering Strait reversal.

2 Background

2.1 Global and Beringian Sea Level during MIS 11

The maximum height of sea level during MIS 11 is an open question with estimates ranging from 6 to 13 m above present sea level (apsl) (Dutton et al., 2015) to 0 m apsl (Rohling et al., 2010; Rohling et al., 2014). The discrepancy may stem from large differences between global eustatic (Bowen, 2010) or ice-volume averages (McManus et al., 2003) and regional geomorphological or micropaleontological evidence (van Hengstum et al., 2009). Regional isostatic adjustment due to glacial loading and unloading are now known to be significant and regional highstands may record higher than expected sea levels if glacial isostasy and dynamic topography have not been accounted for, even in places that were never glaciated (PAGES et al., 2016; Raymo and Mitrovica, 2012; Raymo et al., 2011). For example, Raymo and Mitrovica (2012) suggest eustatic sea level during MIS 11 was 6-13 m apsl globally and near 5 m apsl locally in Beringia, yet MIS 11 shorelines are at +22 m today in northwest Alaska (Kaufman and Brigham-Grette, 1993) due to this complex geophysics.

Regardless of the ultimate height of sea level, the transition from MIS 12 to MIS 11 records the greatest change in sea level of the last 500 ka (Rohling et al., 2014); sea level

rose from perhaps -140 m to its present level or higher (Bowen, 2010)(Dutton et al., 2015). Sea level history during MIS 11 may have been complex (Kindler and Hearty, 2000), but most records agree that sea level during this exceptionally long interglacial (30 kyrs) was highest from 410 to 401 ka, coincident with a second peak in June insolation at 65°N. This long highstand most likely requires partial or complete collapse of the Greenland ice sheet (up to 6 m) (de Vernal and Hillaire-Marcel, 2008; Reyes et al., 2014) and/or the West Antarctic Ice Sheet (Scherer et al., 1998), but not the East Antarctic Ice Sheet (Berger et al., 2015; Dutton et al., 2015; Raymo and Mitrovica, 2012). It has frequently been hypothesized that the West Antarctic Ice Sheet collapsed during MIS 11 and modeling studies confirm this (Pollard and DeConto, 2009), however unconformities in the record prevent confirmation of a collapse (McKay et al., 2012). Yet, Teitler (2015) show that IRD during MIS 11 dropped as low as it was during MIS 31, when it is clear that the West Antarctic Ice Sheet had collapsed (Naish et al., 2009). With uncertainties, East Antarctica ice was stable; however, small changes in either sector of the Antarctic ice sheet may have contributed up to 5 m of sea level rise (Berger et al., 2015; EPICA Community Members, 2004).

The sea level history of Beringia defines Arctic communication between the Pacific and the Atlantic oceans during the Plio-Pleistocene. As a region, Beringia consists of both the terrestrial and marine regions north of the Aleutian Islands that stretch to the shelf-slope break in the Bering, East Siberian, Chukchi, and Beaufort seas (Fig. 1). On land, Beringia extends from the Lena River in Siberia to the Mackenzie River in Canada. Large portions of the Beringian shelf were exposed when sea level dropped below -50 m (Hopkins, 1959) and this subaerial expanse stretches more than 1000 km from north to south during most glacial periods (Fig. 2). In contrast, as sea level rises at glacial terminations the expansive continental shelf is flooded, rapidly once sea level reaches -60 mapsl (Keigwin et al., 2006). This introduces fresh organic matter and nutrients into the southern Bering Sea (i.e. Bertrand et al., 2000; Shiga and Koizumi, 2000; Ternois et al., 2001), re-establishing at -50 mapsl the connection between the Pacific and Atlantic oceans through Bering Strait (Keigwin et al., 2006). The late Cenozoic history of the depth of the Bering Strait sill is poorly known, hence current oceanographic reconstructions (e.g., Knudson and Ravelo, 2015) assume that a sill depth of -50 mapsl was temporally stable, which is

probably not the case and requires future study. However, in this study, we also assume that a sill depth of -50 mapsl controls oceanographic communication between the Atlantic and Pacific Oceans.

2.2 Site Location and Oceanographic Setting

The Integrated Ocean Drilling Program's (IODP) Expedition 323, Site U1345, is located on an interfluve ridge near the shelf-slope break in the Bering Sea (Fig. 1). Navarin Canyon, one of the largest submarine canyons in the world (Normack and Carlson, 2003) is located just to the northwest of the site. Sediments were retrieved from ~1008 m of water, placing the site within the center of the modern day oxygen minimum zone (Takahashi et al., 2011). We focus on this site because of its proximity to the modern marginal ice zone in the Bering Sea and observed high sedimentation rates. Its siting on top of an interfluve was chosen to reduce the influence of turbidites moving through Navarin Canyon.

Today, water circulates cyclonically in the deep basins of the Bering Sea (Fig. 1). Site U1345 is influenced by the northwest flowing Bering Slope Current (BSC), which is derived from the Alaskan Stream (AS). South of the Aleutians Islands, the Alaskan Stream flows westward and enters the Bering Sea through deep channels in the western Aleutian Islands. Once north of the Aleutian Islands, this water mass becomes the Aleutian North Slope Current (ANS), and flows eastward until it reaches the Bering Sea shelf. Interactions with the shelf turn this current to the northwest where it becomes the Bering Slope Current (Stabeno et al., 1999). Tidal forces and eddies in the Bering Slope Current drive upwelling through Navarin Canyon and other interfluves along the shelf-slope break (Kowalik, 1999). The resulting cold water and nutrients brought to the sea surface, coupled with the presence of seasonal sea ice, drive the high productivity found today in the so called "Green Belt" (Springer et al., 1996) along the shelf-slope break. North of the site, low salinity, high nutrient shelf waters (Cooper et al., 1997) primarily flow north through the Bering Strait to the Arctic Basin (Schumacher and Stabeno, 1998).

3 Methods

3.1 Age Model

The age model (Fig. 3) is derived from the shipboard age model, which was developed using magnetostratigraphy and biostratigraphy. First and last appearance datums for diatoms and radiolarians make up the majority of the biostratigraphic markers used to place the record in the correct general stratigraphic position (Takahashi et al., 2011). Oxygen isotope measurements taken on the benthic foraminifera, *Uvigerina peregrina, Nonionella labradorica,* and *Globobulimina affinis* (Cook et al., 2016) were then used to tune site U1345 to the global marine benthic foraminiferal isotope stack (LR04) (Lisiecki and Raymo, 2005) (Fig. 3; Table 1). Based on this combined age model, MIS 11 spans from 115.3 to 130.6 mbsf (Cook et al., 2016); however, the characteristic interglacial isotopic depletion was not found in U1345 which means that the exact timing of peak interglacial conditions is unknown.

The nearby core, IODP Exp 323, Site U1343 (Fig. 1) has an excellent oxygen isotopic record during MIS 11 (Asahi et al., 2016). We compared the two isotopic records and their magnetic susceptibilities (Fig. 3) and found that even with only two tie points, there was good correlation between the timing of the onset of laminated intervals and also the interglacial increase in magnetic susceptibility (Fig. 3b). We added one additional tie point to connect the inflection points in magnetic susceptibility (Table 1). In U1343, this point occurred at 398.50 ka. U1345 was shifted 1.5 ka younger in order to align with U1343. The addition of this point allows us to have more confidence in the timing of peak interglacial conditions in U1345. However, given the oxygen isotope sampling resolution, as well as the stated error in the LR04 dataset (4 kyr), we estimate the error of the age model could be up to 5 kyr. Therefore, we urge caution when comparing millennial scale changes at this site with other sites that examine MIS 11 at millennial scale resolution or finer.

Sedimentation rates during the study interval range from 29 cm/kyrs to 45 cm/kyr with the highest sedimentation rates occurring during glacial periods. Depths and ages of major climate intervals referred to in the text are found in Table 2.

3.2 Sediment Analyses

Details about sediment sampling can be found in the Supplementary Materials. Quantative diatom slides were prepared (Scherer) and counted (Schrader and Gersonde, 1978) using published taxonomic descriptions and images (Hasle and Heimdal, 1968; Koizumi, 1973; Lundholm and Hasle, 2008, 2010; Medlin and Hasle, 1990; Medlin and Priddle, 1990; Onodera and Takahashi, 2007; Sancetta, 1982, 1987; Syvertsen, 1979; Tomas, 1996; Witkowski et al., 2000). Diatom taxa were then grouped according to ecological niche (Table 3) based on biological observations (Aizawa et al., 2005; Fryxell and Hasle, 1972; Håkansson, 2002; Horner, 1985; Saito and Taniguchi, 1978; Schandelmeier and Alexander, 1981; von Quillfeldt, 2001; von Quillfeldt et al., 2003) and statistical associations (Barron et al., 2009; Caissie et al., 2010; Hay et al., 2007; Katsuki and Takahashi, 2005; Lopes et al., 2006; McQuoid and Hobson, 2001; Sancetta, 1982, 1981; Sancetta and Robinson, 1983; Sancetta and Silvestri, 1986; Shiga and Koizumi, 2000). In cases where a diatom species was reported to fit into more than one environmental niche, it was grouped into the niche where it was most commonly recognized in the literature.

Eighteen quantitative calcareous nannofossil slides were prepared (Flores and Sierro, 1997) and counted using a Zeiss polarized light microscope at 1000x magnification. Samples were considered barren if no coccoliths were found in at least 165 randomly selected fields of view. All taxa were identified to the species or variety level (Flores et al., 1999; Young et al., 2003).

Grain size of both biogenic and terrigenous sediment was measured using a Malvern Mastersizer 3000 with the Hydro MV automated wet dispersion unit. The mineralogy of ten samples was analyzed using a Siemens D-5000 X-Ray Diffractometer (Eberl, 2003)

The carbon and nitrogen isotopic and elemental composition of organic matter was determined by Dumas combustion using a Carlo Erba 1108 elemental analyzer coupled to a Thermo-Finnigan Delta Plus XP isotope ratio mass spectrometer at the University of California Santa Cruz Stable Isotope Laboratory. The 1-sigma precision of stable isotope measurements and elemental composition of carbon are 0.2‰ and 0.03%, respectively, and for nitrogen are 0.2‰ and 0.002%, respectively. $\delta^{13}C$ values are reported relative to

207 the Vienna Pee Dee Belemnite (VPDB) and $\delta^{15}N$ values are reported relative to
208 atmospheric N_2. Percent $CaCO_3$ was calculated according to Schubert and Calvert (2001).
209 More detailed methodology can be found in the Supplemental Materials.

210

211 # 4 Results

212 ## 4.1 Sedimentology

213 The sediments at Site U1345 are massive with centimeter–scale dark or coarse-grained
214 mottles. They are mainly composed of clay and silt with varying amounts of diatoms,
215 sand, and tephra throughout. Laminated intervals bracket MIS 11 (Fig. 4). The proportion
216 of diatoms relative to terrigenous or volcanogenic grains is highest during laminated
217 intervals and lowest immediately preceding Termination V (~425 ka). Vesiculated tephra
218 shards were seen in every diatom slide analyzed. Several thin (< 1 cm) sand layers and
219 shell fragments were visible on the split cores, especially during MIS 12. However, high-
220 resolution grain size analyses show that the median grain size was lowest during MIS 12,
221 increasing from approximately 14 μm to 21 μm at the start of Termination V at 424.5 ka
222 (130.92 mbsf). Median grain size peaks at 84 μm between 401 and 407 ka (125.42-
223 123.62 mbsf). This interval is also the location of an obvious sandy layer in the core.
224 After this "anomalous interval," median grain size remains steady at about 17 μm.
225 Subrounded to rounded clasts (granule to pebble) commonly occur on the split surface of
226 the cores. We combined clast and sand layer data from all Holes at Site U1345 when
227 examining their distribution (Fig. 4).

228 A 3.5 m thick laminated interval, estimated to span 12 kyrs (see Table 4 for depths and
229 ages) is deposited beginning during Termination V. Although the termination is short-
230 lived and the laminated interval quite long, we refer to it as the Termination V
231 Laminations for the sake of clarity throughout this manuscript. The next laminated
232 interval occurs at about 394 ka and lasts approximately 1.1 kyrs. During the transition
233 from late MIS 11 to MIS 10, a series of four thin laminated intervals are observed. Each
234 interval lasts between 0.34 and 1.25 ka (Table 4). In general, the upper and lower
235 boundaries of laminated intervals are gradational; however the boundaries between
236 individual lamina are sharp (Takahashi et al., 2011). There are two types of laminations.

The Termination V Laminations are Type I laminations: millimeter-scale alternations of black, olive gray, and light brown triplets. In addition to containing a high proportion of diatoms, this type of laminated interval also contains high relative proportions of calcareous nannofossils and foraminifera (Takahashi et al., 2011). The majority of laminations are parallel; however, a 7 cm interval during the Termination V Laminations is highly disturbed in Hole A, showing recumbent folds in the laminations (Takahashi et al., 2011). This interval was not sampled. Type II laminations occur throughout the remainder of MIS 11. These laminations have fewer diatoms and tend to be couplets of siliciclastic sediments with <40% diatoms (Takahashi et al., 2011). Percent $CaCO_3$ also increases during these laminations though foraminifera and calcareous nannofossils are very rarely seen. None of these later laminated intervals contain any evidence of disturbance.

4.2 Mineralogy

We determined the weight percent of 23 common minerals in ten samples across the study interval. Samples are primarily composed of quartz, plagioclase, tephra, illite and chlorite with minor amounts of other clay and non-clay minerals (Table 5). Downcore, the largest variability occurs in the weight percent of quartz, chlorite, and illite. In general, chlorite comprises nearly 35% of the minerals present in the sediments until 399 ka, and then declines ~ 5% for the remainder of MIS 11. Conversely, quartz increases from 422 to 397 ka and then comprises ~15% of the minerals for the remainder of MIS 11. Illite is lower than 2% of the mineral assemblage at 424 ka, and then increases rapidly to nearly 10% at 422 ka. It remains near 10% for the remainder of MIS 11 except for a brief negative excursion at 397 ka.

4.3 Diatoms

4.3.1 Diatom Assemblages

A total of 97 different diatom taxa were identified. Individual samples include between 26 and 46 taxa each with an average of 37 taxa. Both types of laminated intervals contain fewer taxa than bioturbated intervals do. This decrease in diversity is confirmed using the

Margalef, Simpson, and Shannon indices (Maurer and McGill, 2011) which all show similar down-core profiles (Fig. 5). The Margalef index is a measure of species richness. It shows a decrease in the number of taxa during four out of five laminated intervals that are sufficiently well sampled. Between laminated intervals, there is also a noted decrease in taxa at 388 ka. The Simpson index measures the evenness of the sample. Values close to 1 indicate that all taxa contain an equal number of individuals, while values close to 0 indicate that one species dominates the assemblage. In general, the Simpson index is close to 1 throughout the core; however, during the Termination V Laminations and the most recent two laminations, the Simpson index decreases reflecting the dominance by *Chaetoceros* RS during these intervals (Fig. 5). The Simpson index never approaches 0, which would likely indicate a strong dissolution signal. The Shannon diversity index measures both species richness and evenness. Correspondingly, it is low during three of the laminated intervals, high during MIS 12 and peaks at 397 ka (Fig. 5).

Absolute diatom abundances vary between 10^6 and 10^8 diatoms deposited per gram of sediment with values an order of magnitude higher during most laminated intervals than during massive intervals (Fig. 5). The diatom assemblage is dominated by *Chaetoceros* and *Thalassiosira antarctica* resting spores (RS), with lesser contributions from *Fragilariopsis oceanica, F. cylindrus, Fossula arctica, Shionodiscus trifultus* (=*T. trifulta), T. binata,* small (<10 μm in diameter) *T.* species, *Paralia sulcata, Lindavia* cf. *ocellata*, *Neodenticula seminae,* and *Thalassionema nitzschioides* (Fig. 6).

4.3.2 Qualitative Diatom Proxies

Diatoms, like many organisms, thrive under a specific range of environmental conditions or optima that are different for each species. For this reason, diatom assemblages are excellent paleoceanographic indicators (Smol, 2002). We grouped diatoms with similar environmental niches together (Table 3) to interpret the paleoceanographic sea surface conditions at the Bering Sea shelf-slope break during MIS 12 to 10 (Caissie, 2012; Caissie and Nesterovich, In Prep; Katsuki and Takahashi, 2005; Sancetta, 1982) (Fig. 7). Grouping diverse species together may result in a loss of information when two different species in the same niche show differing abundance patterns over time. On the other

hand, changes in abundances may simply reflect different species filling the same niche at different times.

Chaetoceros resting spores are the dominant taxa included in the high productivity group (Table 3). Relative percent abundances of *Chaetoceros* RS are highest (up to 69%) during the Termination V Laminations and follow the pattern of both diatom accumulation rate and insolation at 65° N (Berger and Loutre, 1991). The lowest relative abundances (15-20%) of *Chaetoceros*/high productivity species occur between 403 and 390 ka (124.21 to 120.07 mbsf) when both obliquity and insolation are low (Fig. 7h).

Epontic diatoms are those that bloom attached to the underside of sea ice or within brine channels in the ice (Alexander and Chapman, 1981). This initial bloom occurs below the ice as soon as enough light penetrates to initiate photosynthesis in the Bering Sea, which can occur as early as March (Alexander and Chapman, 1981). A second ice-associated bloom occurs as sea ice begins to break up on the Bering Sea shelf. This bloom is referred to as the marginal ice zone bloom and many of its members are common species in the sediment assemblage. Several diatom species are present in both types of sea ice blooms, and so while they are indicators of ice presence, they cannot be used to distinguish between types of sea ice. These species are grouped under "both ice types" (Table 3).

Epontic species are present in very low relative percent abundances (< 1%) throughout much of the record, present only when fresh water diatoms also increase (Fig. 7i, 7n). Marginal ice zone species fluctuate between 4% and 14% throughout the record and do not show any trends in abundance changes (Fig. 7j). The grouping of species found both within the ice and in the water surrounding ice, however, is also somewhat reduced during laminated intervals (Fig. 7k).

A cold layer of water found between seasonally warmer surface and warmer deep water characterizes dicothermal water. It is stable because of its very low salinity. In the Sea of Okhotsk and the Bering Sea today, the dicothermal layer is associated with melting sea ice. Genera present in the Bering Sea during late summer tend to co-vary with the dicothermal water indicators, so the two groups were merged for comparison with other diatom groups. *S. trifultus* is the dominant species in the dicothermal group (Table 3). It

is relatively high (~4%) during MIS 12, is virtually absent from the sediments during the Termination V Laminations, and then increases again until it peaks at 10% relative abundance at 400 ka (123.22 mbsf) (Fig. 6).

Neritic species maintain ~10% relative abundance throughout the core (Fig. 7m). The dominant species in the neritic group is *Paralia sulcata* (Table 3), sometimes considered an indicator of shallow, moving water (Sancetta, 1982). Neritic species are lowest during the Termination V Laminations and increase dramatically around 404 ka (124.61 mbsf) to almost 50% of the assemblage (Fig. 7n). *L.* cf. *ocellata* is the dominant taxa in the fresh water group. This group is notably absent from much of the core, but prevalent between 401 and 392 ka (123.70 mbsf and 121.20 mbsf); it reaches its highest relative percent abundance (12%) at 401 ka (123.62 mbsf) (Fig. 7n).

Neodenticula seminae is used here as a tracer of Pacific water (Caissie et al., 2010; Katsuki and Takahashi, 2005). Absolute abundances begin to increase at 422 ka as global eustatic sea level rises above -50 mapsl. Abundance then decreases slowly over the course of the Termination V Laminations and peaks again at 392 ka and 382 ka. As sea level drops below -50 mapsl, *N. seminae* is no longer present at U1345. Relative percent abundances remain stable at ~2% relative percent abundance between 422 and 400 ka (129.62-123.62 mbsf), then peak at 13% at 392 ka (121.22 mbsf) (Fig. 6 and 7o).

Diatoms associated with warmer water or classified as members of temperate to subtropical assemblages (Table 3) are quite low throughout the record (<5%), and are highest (3-4%) during mid to late MIS 11 approximately ~410 to 391 ka (126.74 to 116.50 mbsf) (Fig. 7p).

4.4 Calcareous Nannofossils

Calcareous nannofossils were examined between 432-405 ka (133.4 to 125.0 mbsf); one third of the samples were barren (Fig. 7g, open purple circles) and only one sample (418 ka; 128.8 mbsf) had sufficient individuals to estimate relative percent abundances (Fig. 7g). This sample is located midway through the Termination V Laminations when the diatom assemblage is overwhelmingly dominated by *Chaetoceros* RS. Small

Gephyrocapsa dominates (>50%) the calcareous nannofossil assemblage. There are 35% medium *Gephyrocapsa,* 9% *Coccolithus pelagicus*, and 1% *Gephyrocapsa oceanica*.

4.5 Geochemistry

4.5.1 Organic and Inorganic Carbon Content

Total organic carbon (TOC) roughly follows the trend of relative percent abundances of *Chaetoceros* RS, with higher values during the Termination V Laminations (Fig. 7b, 7h). Mean TOC value during MIS 12 is 0.76%, and during the Termination V Laminations, it is 1.11%. TOC decreases between 408 (125.82 mbsf) and 404 ka (124.77 mbsf) coeval with a decrease in $\delta^{15}N$ values. After 404 ka, it increases linearly to 374 ka (115.39 mbsf). TOC is again high during the late MIS 11/MIS 10 laminations.

In contrast, inorganic carbon, calculated as % $CaCO_3$ is less than 1% for most of the record (Fig. 7g). However, it increases up to 3.5% during the laminated intervals and also at 382 ka (117.87 mbsf), 392 ka (110.00 mbsf), and 408 ka (125.82 mbsf).

4.5.2 Terrigenous vs. Marine Input Indicators

Nitrogen, carbon and their isotopes can be used to determine relative amounts of terrigenous vs. marine organic mater input. Total nitrogen (TN) is significantly correlated with total organic carbon (TOC) (Fig. 8a); however, the y-intercept of a regression line through the data is 0.03 (Fig. 8a), indicating that there is a significant fraction of inorganic nitrogen in the sediments (Schubert and Calvert, 2001). Inorganic nitrogen can be adsorbed onto clay particles or incorporated into the crystal lattice of potassium-rich clays such as illite. This complicates interpretations of elemental nitrogen and its isotopes because the presence of inorganic nitrogen will lower C_{org}/N ratios and $\delta^{15}N$ values (Muller, 1977; Schubert and Calvert, 2001).

Bearing this bias in mind, the relative terrigenous contribution to the sediments can be estimated by examining where U1345 samples plot in relation to typical C_{org}/N, $\delta^{15}N$, and $\delta^{13}C$ values for marine phytoplankton, refractory soil organic matter, and C3 vascular plants (Fig. 8). Note that we use N/C_{org}, the inverse of C_{org}/N, because we seek to derive

the terrigenous carbon fraction rather than the fraction of terrigenous nitrogen (Perdue and Koprivnjak, 2007). Throughout MIS 12-10, organic matter is comprised of a mixture of marine and terrigenous organic matter. There is a higher contribution of marine organic matter during MIS 12, 10, and between 394 and 405 ka and a higher contribution of terrigenous organic matter during peak MIS 11 (Fig. 8). The N/C_{org} ratio indicates that during peak MIS 11, this terrigenous organic matter is likely refractory soil organic matter, rather than fresh vascular plant organic matter (Fig. 8b).

During MIS 12, C_{org}/N is highly variable, when sea level is below -50 m apsl (Fig. 7). As sea level rises during Termination V, C_{org}/N values increase from 6 to more than 9. The highest C_{org}/N value occurs at the start of the Termination V Laminations. C_{org}/N decreases as sea level rises until at 400 ka (123.62 mbsf) it stabilizes near 7 for the remainder of the record (Fig. 7).

Carbon isotopic values range between -22 ‰ and -26 ‰. No sample has low enough $\delta^{13}C$ values to be comprised fully of typical Arctic Ocean marine phytoplankton (-22 to -19‰) or ice-related plankton (-18.3‰) (Schubert and Calvert, 2001); however samples from MIS 10, MIS 12, and the "anomalous interval" all plot close to marine phytoplankton values (Fig. 8b). At the onset of the Termination V Laminations, $\delta^{13}C$ becomes more negative and then gradually increases to a maximum of -22.33 at 404 ka (124.62). After 400 ka (123.5 mbsf), $\delta^{13}C$ is relatively stable around -23.5‰ (Fig 7).

4.5.3 Nitrogen Isotopes

The nitrogen isotopic composition of bulk marine sediments can be thought of as a combination of the $\delta^{15}N$ of the source nitrate and the amount of nitrogen utilization by phytoplankton (Brunelle et al., 2007). Denitrification is common in the low oxygen waters of the eastern tropical North Pacific (Liu et al., 2005) and in the Bering Sea during the Bølling-Allerød (Schlung et al., 2013), leading to enriched core top $\delta^{15}N$ values between 8 and 9‰. When diatoms utilize nitrogen, they preferentially assimilate the lighter isotope, ^{14}N, which enriches surface waters with respect to ^{15}N (Sigman et al., 1999). Complete nitrogen utilization would result in $\delta^{15}N$ values identical to that of the source nitrate (Sigman et al., 1999). Sponge spicules (very low $\delta^{15}N$ values) and

radiolarians (highly variable $\delta^{15}N$ values) may contaminate the $\delta^{15}N$ of bulk organic matter; therefore, we looked for and found no correlation between spicule abundance and $\delta^{15}N$ in our samples.

$\delta^{15}N$ is relatively stable, but quite high throughout the study interval, fluctuating around an average value of 6.4‰ and reaching values greater than 7‰ and up to 8‰ several times (Fig. 7). There are several notable excursions from these high values. Coeval with sea level rise and increased relative percent *Chaetoceros* RS, $\delta^{15}N$ decreased 2.7‰ to 4.4‰ before recovering to average values during the Termination V Laminations. Two other depletions occur at 405 ka (124.77 mbsf) and 393 ka (121.62 mbsf), the first is the most extreme and reaches 2.9‰.

5 Discussion

5.1 Orbital-Scale Changes in Productivity and Sea Ice

The observed changes in diatom assemblages and lithology (Fig. 7) allow us to break the sedimentary record into five zones: MIS 12, Termination V, Peak MIS 11, Beringian Glacial Initiation, and Late MIS 11 (Table 2). These zones reflect changing sea ice, glacial ice, sea level, and SST and correspond to events recognized elsewhere in ice cores and marine and lake sediments.

5.1.1 Marine Isotope Stage 12 and Early Deglaciation (431-425 ka)

From 431 to 425 ka, the record chronicles conditions at the end of MIS 12. Although diatom accumulation rate is quite low, a relatively diverse assemblage characterizes this period (Fig. 5) with moderate amounts of sea ice, high productivity, and dicothermal species (Fig. 7), indicating seasonal sea ice with highly stratified waters during the ice-melt season. Nitrogen isotopes indicate high nutrient utilization (Fig. 7) consistent with nitrogen-limited productivity in stratified waters as well as localized denitrification. Numerous shell fragments, two sand layers and the highest percentages of clay-sized sediments in the record were deposited during MIS 12 (Figs 4 and 8) indicating input of terrigenous material, however, crossplots of elemental (C_{org}/N or N/C_{org}) and isotopic

($\delta^{13}C$, $\delta^{15}N$) indicators of terrigenous and marine carbon pools indicate that the organic matter during MIS 12 is a diverse mix of marine phytoplankton and soil detritus (Fig. 8) likely derived from in-situ, but low, productivity and transport by several methods including large, oligotrophic rivers and downslope transport. Glacial ice was likely restricted to mountain-valley glaciers, similar to the last glacial maximum (e.g. Glushkova, 2001). These small, distant glaciers would not have produced large amounts of ice bergs though occasional glacial ice rafted debris (IRD) may have come from the Koryak Mountains, the Aleutians or Beringia. Consistent with this, sediments typical of glacial IRD, such as dropstones, are sparse, but present. In addition, sea ice rafting tends to preferentially entrain clay and silt (Reimnitz et al., 1998) and is likely to be an important contributor of terrigenous sediments.

5.1.2 Termination V (425-423 ka)

Termination V is the transition from MIS 12 to MIS 11. Worldwide, it is a rapid deglaciation that is followed by a long (up to 30 kyrs) climate optimum (Milker et al., 2013). At U1345, gradually increasing productivity coupled with decreasing nutrient utilization and sea ice occurs between 425 and 423 ka. This is seen as an increase in absolute diatom abundances and relative percent abundance of *Chaetoceros* RS and a decrease in sea ice diatoms and $\delta^{15}N$ values (Fig. 7). It is plausible that increased nitrogen availability drove higher primary productivity as floods scoured fresh organic matter from the submerging continental shelf (Bertrand et al., 2000). Rapid input of bioavailable nitrogen as the shelf was inundated has been suggested to explain increasing productivity during the last deglaciation in the Sea of Okhotsk (Shiga and Koizumi, 2000) and during MIS 11 in the North Atlantic (Poli et al., 2010) and also may have contributed to dysoxia by ramping up nutrient recycling, bacterial respiration, and decomposition of organic matter in the Bering Sea.

5.1.3 Peak MIS 11 (423-394 ka)

Globally, peak interglacial conditions (often referred to as MIS 11.3 or 11c) are centered around 400 to 410 ka (Dutton et al., 2015; Raymo and Mitrovica, 2012), though the exact interval of the temperature optimum varies globally and lasted anywhere from 10 to 30 kyrs (Kandiano et al., 2012; Kariya et al., 2010; Milker et al., 2013). At U1345, peak interglacial conditions begin during the Termination V Laminations at 423 ka and continue until 394 ka, lasting nearly 30 kyrs consistent with the synthesis of the PAGES Past Interglacials working group (2016).

5.1.3.1 Laminations (423-410 ka)

A 3.5 m thick laminated interval is deposited during early MIS 11 beginning at 423 ka (Fig. 7) when insolation was high at 65°N (Berger and Loutre, 1991). Its presence indicates that the bottom water at 1,000 m in the Bering Sea was dysoxic for more than 11 kyrs. These laminations are characterized as Type I laminations with a high diatom content (Fig. 4). Several lines of evidence point towards high productivity among multiple phytoplankton groups as opposed to simply a change in preservation. First, we see an increase in diatom abundances by two orders of magnitude increase since MIS 12, second, a low-diversity diatom assemblage dominated by *Chaetoceros* RS, third, an abrupt increase in percent organic carbon, and fourth, high percent $CaCO_3$ and abundant calcareous nannofossils dominated by small *Gephyrocapsa.* Furthermore, enriched $\delta^{15}N$ values indicate either increased nitrogen utilization that likely led to this increased productivity or localized denitrification in low oxygen waters (Fig. 7).

Sea ice extent decreases during this interval with no epontic diatoms present and reduced amounts of sea ice diatoms found in both epontic and marginal ice (Fig. 7). Geochemical crossplots indicate a high contribution from soil detritus and C3 plant organic matter (Fig. 8). At the onset of the laminated interval (423 ka), $\delta^{13}C$ decreases and C_{org}/N increases rapidly (Fig. 7) as the tundra-covered Bering Sea shelf is flooded.

However, the diatom record during the laminated interval has the lowest contribution of neritic diatoms and virtually no fresh water diatoms (Fig. 7), suggesting that although

499 terrigenous organic matter was an important input at the site, coastal, river, or
500 swamp/tundra diatoms were not carried out to U1345 with this terrigenous organic
501 matter.

502

503 #### 5.1.3.2 Post Laminations (410-394 ka)

504 Both high N/C_{org} and $\delta^{13}C$ indicate that input of terrigenous organic matter is highest at
505 the onset of the Termination V Laminations and then declines until mid MIS 11 (400 ka)
506 at which time the organic matter is largely derived from marine phytoplankton (Fig. 7;
507 red to grey dots in Fig. 8). This may be related to rising eustatic sea level causing the
508 migration of the paleoshoreline farther northward and away from U1345.

509 Throughout MIS 11, *Chaetoceros* RS, a species indicative of high productivity, is
510 generally higher when insolation is higher and lower when isolation is lower (404-390
511 ka; Fig. 7). However, although their fluctuations are small, warm water species show the
512 opposite trend, with higher proportions of warm water diatoms when insolation is low
513 (Fig. 7). If higher proportions of warm water diatoms indicate warmer water, then this
514 suggests that productivity is highest in colder waters but when insolation is high, and
515 lowest in warmer waters when insolation is low. This may reveal a relationship between
516 upwelling of colder waters and high productivity.

517

518 ### 5.1.4 Late MIS 11 to MIS 10 (younger than 394 ka)

519 After 394 ka, diatom productivity indicators are the lowest in the record but linearly
520 increase to the top of the record. This is in contrast to a slight increase in diatom
521 abundance, which increases at 393 ka and then remains relatively stable into MIS 10. Sea
522 ice indicators also remain relatively high from 392 to the top of the record and
523 dicothermal species reflect moderately stratified waters. Warm water species decrease
524 from 390 ka to the top of the record (Fig. 7). The sum of this evidence indicates that at
525 the end of MIS 11, summers were warm and sea ice occurred seasonally, perhaps lasting
526 a bit longer than at other times in the record.

Eustatic sea level decreased beginning about 402 ka (Rohling et al., 2010), but sea level remained high enough to allow *N. seminae* to reach the shelf slope break until about 380 ka (Fig. 7).

5.2 The Bering Sea in the Context of Regional and Global Variability

Across the Bering Sea, sediments at sites near Bowers Ridge (Fig. 1) are dominated by opal during MIS 11 (Kanematsu et al., 2013); whereas, biogenic sediments at sites along the Bering Slope, including U1345, are diluted by sea ice transport of lithogenic sediments as well as down-slope sediment transport (Kanematsu et al., 2013). However, the rate of biogenic opal accumulation is comparable for all sites in the Bering Sea, despite differences in sedimentation rates (Kanematsu et al., 2013; Stroynowski et al., 2015). Opal content in the sediments varies on glacial/interglacial time scales with high productivity during interglacials. Indeed, the highest percent opal concentration of the past 1 Ma occurs during MIS 11 at the two slope sites, U1345 and U1343 (Kanematsu et al., 2013).

Biogenic opal increases during early MIS 11 at Sites U1343 and U1345 (Kanematsu et al., 2013). At U1345, it mimics the pattern of relative percent abundance of *Chaetoceros* RS, the most abundant productivity indicator (Fig. 9). Although diatom data from other cored sites is low resolution (1-4 samples during MIS 11) (Kato et al., 2016; Onodera et al., 2016; Stroynowski et al., 2015; Teraishi et al., 2016), it provides a snapshot of diatom assemblages during MIS 11. Sea ice diatoms contribute approximately 30% of the diatom assemblages at the two slope sites, U1345 (this study) and U1343 (Teraishi et al., 2016), between 10 and 20% of the assemblage at the eastern Bowers Ridge site (U1340) (Stroynowski et al., 2015), but less than 2% of the assemblage on the western flanks of Bowers Ridge (U1341) (Onodera et al., 2016). In the North Pacific (ODP Site 884), no sea ice diatoms are present during MIS 11 (Kato et al., 2016). Site U1341 contained an assemblage high in dicothermal indicators such as *Shionodiscus trifultus,* and *Actinocyclus curvatulus,* oceanic front indicators such as *Rhizosolenia hebetata,* and *N. seminae* (Onodera et al., 2016), while the North Pacific (Site 884) assemblage is dominated by dicothermal indicators during MIS 11(Kato et al., 2016). Percent opal

declines at Bowers Ridge during early MIS 11 at the same time as it increases at the slope sites (Iwasaki et al., 2016) (Fig. 9) when sea ice is reduced and upwelling along the shelf-slope break is increased. This implies that the relationship between productivity and sea ice in the Bering Sea is perhaps more complex than the simple idea that sea ice inhibits productivity (Iwasaki et al., 2016; Kim et al., 2016). The region is strongly influenced by winter sea ice throughout MIS 11 with seasonal sea ice present farther south along the slope than today and also in the eastern Bering Sea. Highly stratified waters, perhaps due to the seasonal expansion and retreat of sea ice, extended across the entire basin and even into the North Pacific.

Local ventilation of North Pacific Intermediate Water decreased as Bering Strait opened during Termination V with the weakest ventilation occurring around 400 ka (Knudson and Ravelo, 2015). This is coeval with the highest relative percent abundances of dicothermal diatoms indicating highly stratified water (Fig. 9).

5.2.1 Temperature and Aridity during MIS 11

When sea level was low during glacial periods such as MIS 12 (Rohling et al., 2010), U1345 was proximal to the Beringian coast (Fig. 2). With the Bering land bridge exposed, the continent was relatively cold and arid (Glushkova, 2001). In western Beringia, Lake El'gygytgyn was perennially covered with ice, summer air temperatures were warming in sync with increasing insolation from 4 to 12° C, but annual precipitation was low (200-400 mm) (Vogel et al., 2013).

As sea level rose, and global ice volume reached the lowest amount for the past 500 kyrs (Lisiecki and Raymo, 2005), the generally continental temperatures in the Northern Hemisphere increased (D'Anjou et al., 2013; de Vernal and Hillaire-Marcel, 2008; Lozhkin and Anderson, 2013; Lyle et al., 2001; Melles et al., 2012; Pol, 2011; Prokopenko et al., 2010; Raynaud et al., 2005; Tarasov et al., 2011; Tzedakis, 2010; Vogel et al., 2013) with a northward expansion of boreal forests in Beringia (Kleinen et al., 2014). However, the marine realm does not reflect this warming as strongly. At U1345, the relative percent warm water species suggest that SSTs during peak MIS 11 were only slightly warmer than during MIS 12. Indeed, MIS 11 is not the warmest

interglacial in most marine records (Candy et al., 2014), rather MIS 5e is the warmest many places (PAGES et al., 2016). This is especially evident in the Nordic Seas where MIS 11 SSTs were lower than Holocene values (Bauch et al., 2000). However, MIS 11 is unique because it was much longer than MIS 5e in all records (PAGES et al., 2016). One exception to this is the Arctic Ocean, which was warm enough during MIS 11 to imply increased Pacific water input through Bering Strait (Cronin et al., 2013).

With elevated sea level, peak MIS 11c was very humid in many places. In the Bering Sea, modeling studies estimate up to 50 mm more precipitation than today at 410 ka (Kleinen et al., 2014). The most humid, least continental period recorded in the sediments at Lake Baikal occurs from 420-405 ka (Prokopenko et al., 2010), and extremely high precipitation is recorded at Lake El'gygytgyn on the nearby Chukotka Peninsula from 420-400 ka (Melles et al., 2012).

5.2.2 Millennial-Scale Laminations and Changes in Sea Ice

Globally, late MIS 11 is characterized as a series of warm and cold cycles (Candy et al., 2014; Voelker et al., 2010), though there is no agreement on the timing of these cycles. At Site U1345, laminations are deposited intermittently between 394 and 392 ka and again after 375 ka (Fig. 4) as the climate transitioned into MIS 10. These laminations are quite different from the Termination V Laminations due to their shorter duration and lack of obvious shift in terrigenous vs. marine carbon source. In addition, these Type II laminations have higher diatom abundances and $CaCO_3$, but lack increased upwelling indicators. Primary production during these laminations is likely not driven by nutrient upwelling along the shelf-slope break. Instead, most of these laminations show an increase in sea ice diatoms and roughly correspond with millennial scale stadial events that occurred during late MIS 11 in the North Atlantic (Fig. 9) (Voelker et al., 2010) as well as carbonate peaks at Blake Ridge (Chaisson et al., 2002). This suggests teleconnections between the Bering Sea and the North Atlantic at this time and places an indirect constraint on the depth of the Bering Strait sill.

It is possible to note that the laminations occur at a time when global sea level was fluctuating near the sill depth of Bering Strait (-50 m apsl) (Rohling et al., 2010) (see

grey line at -50 m on Fig. 9). When sea level fluctuates near this level, Bering Strait modulates widespread climate changes that see-saw between the Atlantic and Pacific regions on millennial-scale time frames (Hu et al., 2010). And when Bering Strait is closed, North Pacific Intermediate Water formation increases (Knudson and Ravelo, 2015). Further study will elucidate these connections.

A "Younger Dryas-like" temperature reversal is seen midway through Termination V in the North Atlantic (Voelker et al., 2010), Antarctica (EPICA Community Members, 2004) and at Lake El'gygytgyn (Vogel et al., 2013), however there is no evidence for such an event in the Bering Sea.

5.2.3 Anomalous Interval (405-394 ka)

The interval between 405 and 394 ka contains a number of unusual characteristics. Diatom assemblages are similar to those found in nearshore sediments from the Anvillian Transgression 800 km northeast of U1345 in Kotzebue Sound (Fig. 1) (Pushkar et al., 1999). A large peak in neritic species occurs at 404 ka followed by the highest relative percentages of fresh water species at the site and a slight increase in sea ice diatoms from 400 to 394 ka (Fig. 7, grey bar). Primary productivity was low during this interval with the highest $\delta^{15}N$ values of MIS 11, likely indicating denitrification. However, two large depletions in $\delta^{15}N$ bracket this interval and occur as *Chaetoceros* RS decrease in relative percent abundance (Fig. 10). The organic matter is primarily sourced from marine phytoplankton, similar to the organic matter found during the two glacial intervals and distinctly different from the organic matter found during the rest of peak MIS 11 (Fig. 8). Detailed grain size analysis shows a fining upward trend of clay sized grains as well as a broad increase in sand sized grains and in particular grains greater than 250 μm (Fig. 10). All samples are poorly to very poorly sorted (See Supplemental Material). Shipboard data shows an increase in the presence of pebbles, several sand layers (Fig. 10), and a thick interval of silty sand (Takahashi et al., 2011) at 404 ka (Fig. 4). While the presence of coarse material implies a terrestrial source for the sediments during this interval, this terrestrial matter must have been largely devoid of organic matter. The sum of this evidence leads us to investigate further three different interpretations of the interval

highlighted in grey on Fig. 10: a reversal of flow through Bering Strait, a tidewater glacial advance, and a turbidite.

5.2.3.1 Reversal of Bering Strait Through Flow

As sea level rose after MIS 12, the connection between the Pacific and the Atlantic was reestablished via Bering Strait. De Boer and Nof (2004) suggest that under high sea level conditions, if freshwater is suddenly released into the North Atlantic, the Bering Strait might act as an "exhaust valve" allowing fresh water from the Arctic Basin and the North Atlantic to flow into the Arctic Ocean and then flow south through the Bering Strait, thus preventing a shut-down in thermohaline circulation (DeBoer and Nof, 2004).

On St. Lawrence Island (Fig. 1), evidence for Arctic mollusks entering the Gulf of Anadyr suggests that flow through Bering Strait was reversed at some point during the Middle Pleistocene (Hopkins, 1972). Unfortunately, this event is poorly dated.

If flow were reversed due to a meltwater event (DeBoer and Nof, 2004), we would expect a temporary reduction in North Atlantic Deep Water (NADW) formation and an increase in southerly winds from Antarctica (DeBoer and Nof, 2004). In the Bering Sea, we would expect to see an increase in common Arctic or Bering Strait diatom species and a decrease in North Pacific indicators. In addition, the clay minerals in the Arctic Ocean are overwhelmingly dominated by illite (Ortiz et al., 2012), which tends to adsorb large amounts of ammonium (Schubert and Calvert, 2001). So, if net flow were to the south, one might expect to find increased illite and decreased C_{org}/N and $\delta^{15}N$ values.

Proxy evidence for NADW ventilation indicates that between 412 and 392 ka, NADW formation decreased for short periods (< 1 ka) (Poli et al., 2010). In contrast, AABW formation appears to have drastically slowed around 404 ka, suggesting a decrease in sea ice and winds from around Antarctica as the sourthern hemisphere warmed (Hall et al., 2001).

At U1345, diversity is highest around 400 ka, due to the multiple contributions of Arctic species (fresh water, shelf, coastal, sea ice) and common pelagic diatoms, while the North Pacific indicator, *N. seminae* maintains low relative abundances and does not change throughout this interval. No marked increase in illite is observed during this interval in

either U1345 or elsewhere on the Bering Slope (Kim et al., 2016) (Fig. 9). However, chlorite, which dominates North Pacific sediments (Ortiz et al., 2012) decreases at 399 ka (Fig. 9), suggesting a reduced Pacific influence. C_{org}/N values began decreasing linearly starting at 409 ka, productivity sharply decreases at 406 ka, $\delta^{15}N$ values are the most depleted at 405 ka, just 1 kyr before a conspicuous peak in *P. sulcata,* a common diatom found in the Bering Strait. Because there is conflicting evidence of both northward and southward flow, we reject the hypothesis of reversed flow through Bering Strait during MIS 11.

5.2.3.2 Glacial Advance

At its maximum, the Nome River Glaciation is the most extensive glaciation in central Beringia and is dated to Middle Pleistocene. Although it has not been precisely dated, it is likely correlative with late MIS 11 or MIS 10 (Kaufman et al., 1991; Miller et al., 2009). Nome River glaciomarine sediments recording the onset of rapid tidewater glacial advance are found in places such as St. Lawrence Island (Gualtieri and Brigham-Grette, 2001; Hopkins, 1972), the Pribilof Islands (Hopkins, 1966), the Alaska Arctic coastal plain (Kaufman and Brigham-Grette, 1993), Kotzebue (Huston et al., 1990), Nome (Kaufman, 1992), and Bristol Bay (Kaufman et al., 2001) (Fig. 1). At these sites glaciers advanced, in some cases more than 200 km, and reached tidewater while eustatic sea level was high (Huston et al., 1990).

Although global sea level was near its maximum, and much of the world was experiencing peak MIS 11 conditions (Candy et al., 2014), there is evidence that the high latitudes were already cooling. At 410 ka, insolation at 65° N began to decline (Berger and Loutre, 1991), and cooling began at 407 ka in Antarctica, expressed both isotopically and as an expansion of sea ice (Pol, 2011). Millennial scale cooling events were recorded at Lake Baikal (Prokopenko et al., 2010). By 405 ka, there was some evidence globally for ice sheet growth (Milker et al., 2013) as Lake Baikal began to shift towards a dryer, more continental climate (Prokopenko et al., 2010) and productivity declined at Lake El'gygytgyn (Melles et al., 2012).

706 Solar forcing coupled with a proximal moisture source, the flooded Beringian shelf,
707 drove snow buildup (Brigham-Grette et al., 2001; Huston et al., 1990; Pushkar et al.,
708 1999) and glacial advance from coastal mountain systems. Precipitation at Lake
709 El'gygytgyn, just west of the Bering Strait, was two to three times higher than today at
710 405 ka(Melles et al., 2012). A similar "snow gun" hypothesis has been invoked for other
711 high latitude glaciations (Miller and De Vernal, 1992); however, Beringia is uniquely
712 situated. Once sea level began to drop, Beringia became more continental and arid
713 (Prokopenko et al., 2010) and the moisture source for these glaciers was quickly cut off.

714 Subaerial and glaciofluvial deposits below the Nome River tills and correlative
715 glaciations indicate that Beringian ice, especially from the western Brooks Range,
716 advanced as the climate grew colder. Ice wedges and evidence of permafrost are common
717 (Huston et al., 1990; Pushkar et al., 1999) in sand and gravel deposits later overridden by
718 Nome River till.

719 If evidence of the Nome River glaciation in central Beringia was present at U1345, we
720 might expect to see evidence of glacial ice rafting. Previous work has suggested that
721 sediments deposited by icebergs should be poorly sorted and skew towards coarser
722 sediments (Nürnberg et al., 1994). Sediments greater than 150 μm are likely glacially ice
723 rafted (St. John, 2008), however it is not possible to distinguish sediments deposited by
724 glacial versus sea ice on grain size alone (St. John, 2008). Both types of ice commonly
725 carry sand-sized or larger sediments (Nürnberg et al., 1994). Sea ice diatoms should not
726 be found in glacial ice, instead, we would expect glacial ice to be either barren, or to
727 carry fresh water diatoms from ice-scoured lake and pond sediments. At U1345, there is a
728 brief coarse interval (405-402 ka) followed by deposition of fresh water diatoms until 394
729 ka.

730 Although it is tempting to assign this to the Nome River Glaciation, there are too many
731 unknowns including whether the coarse grains were transported by sea ice, glacial ice, or
732 some other method. Further work is ongoing to look for the onset of the Nome River
733 Glaciation in both MIS 11 and MIS 13 as well as to distinguish the transport mechanism
734 for these quartz grains.

735

5.2.3.3 Turbidite

The location of Site U1345 on a high interfluve was chosen to minimize the likelihood that sediments could have been transported and deposited here by turbidites or other down-slope currents, yet evidence for a turbidite during this interval is very strong. Although there is no evidence of slumping or distorted sediments, clear erosive surfaces, or any structures that would indicate a turbidite during the anomalous interval, there are folded laminations elsewhere in the sediment core (Takahashi et al., 2011). If this interval was a turbidite, we would expect an erosive surface, overlain by clasts and perhaps a coarse sand layer followed by a fining up sequence. We see intermittent sand layers and small pebbles coupled with a linear increase in the percent clay throughout the interval (Fig. 10). Sediments are poorly sorted throughout the interval, consistent with rapid turbidite deposition and the presence of neritic and fresh water diatoms suggest redeposition of these sediments offshore from shallow water. Sancetta and Robinson (1983) argue that benthic pennate species were transported out of shallow water by rivers and turbidity currents during glacial periods; however, they do not consider ice as a transport mechanism. In this study, we have considered most benthic pennate species as members of either the epontic or both ice ecological niches (von Quillfeldt et al., 2003). However, it is striking that the pattern of benthic pennate species at U1345 is nearly identical to that of the fresh water species.

Although the evidence is strongest for a turbidite, it is unusual to find just one turbidite as we might expect a turbidity flow to exist in the same place for a prolonged period. Further investigation of this and other Bering Sea cores can elucidate how common intervals like this are along the slope and if there is temporal consistency between deposits. The presence of a turbidite may suggest that the age model for this core needs to be slightly revised; however, there is no evidence of an erosive surface, nor a clear indication that all of the material deposited during this interval is allochthonous. In addition, the presence of a turbidite does not change the overall orbital and millennial scale interpretations of this record. Therefore, we choose to keep the age model as is.

6 Conclusions

This study aimed to describe orbital- and millennial-scale changes in productivity and sea ice extent in the Bering Sea, specifically at the shelf-slope break Site U1345. We further tested two hypotheses: 1) in Beringia, tidewater glaciers advanced while sea level was high and 2) Bering Strait Through Flow reversed shortly after the MIS 12 glacial termination (Termination V).

The interval between MIS 12 and MIS 10 is marked by large changes in productivity but only minor changes in sea ice extent at Site U1345. Productivity changed in concert with changes in insolation and water temperature. During warmer periods, high stratification appears to have led to lowered productivity. Site U1345 sites in the present-day oxygen minimum zone, and the presence of laminations frequently throughout the core indicates that oxygen is low. Evidence of denitrification is prevalent for much of the record, likely due to dysoxic conditions.

During MIS 12, productivity was low and seasonal sea ice dominated the Bering Sea with highly stratified waters during the ice-melt season. At Termination V, diatom productivity increased by two orders of magnitude while nitrogen utilization decreased. At 423 ka, an 11 kyr long laminated interval began. This interval was highly productive for multiple phytoplankton groups. The surface waters were relatively unstratified, and sea ice, though still present, decreased. This period is marked by the highest terrigenous organic matter input of the record possibly due to scouring of the continental shelf as sea level rose. During peak and late MIS 11, SSTs appear to have been warm, but seasonal sea ice lasted longer. And at the end of MIS 11, sea ice increased as sea level declined.

Laminations at the end of MIS 11 correspond with millennial scale stadials seen in the N Atlantic. These deposits represent possible evidence of teleconnections between the Atlantic and the Pacific as eustatic sea level fluctuated near the Bering Strait sill depth.

Decreased NADW formation and species transport from the Arctic Ocean southward support a reversal of the Bering Strait Current at 405 ka; however, there is no evidence for the transport of Arctic Ocean clay minerals or oceanographic forcing related to an increase in winds in Antarctica. Therefore, there is inconclusive evidence for a reversal of the Bering Strait Current during MIS 11.

When global sea level was at its maximum, insolation dropped and Beringia began to cool in sync with other polar regions. Sediments deposited during the so called, "anomalous interval" may have been carried by tidewater glaciers bringing neritic species far off shore. This glacial advance is attributed to humid conditions in Beringia that allowed rapid glacial growth. Alternatively, this interval may be a turbidite which could shift the age model for this core and cause this section to be omitted from the paleoceanographic record.

Previous studies have referred to MIS 11 as an analog for the next century of climate change. Today sea ice barely reaches Site U1345 even in winter and does not reach any other Bering Sea or North Pacific sites (U1340, U1341, U1343 or ODP 884). In contrast, during MIS 11, sea ice diatoms are present throughout the entirety of MIS 11 at U1345 and seasonal sea ice appears to have reached both slope sites and the eastern Bowers Ridge (Onodera et al., 2016; Stroynowski et al., 2015; Teraishi et al., 2016). However, evidence for a reduction of sea ice in the Arctic Ocean during MIS 11 (Cronin et al., 2013) implies that while winter sea ice was expanded in the Bering Sea compared to today, summer sea ice was likely reduced. Such a significant difference may indicate that MIS 11 is not an ideal analog for climate change over the next 100 years.

However, there are lessons to be learned from the paleo-record. When sea ice declined during early MIS 11, nutrients were upwelled from the deep Bering Sea and flooding of the land bridge further brought nutrients into the surface waters. This caused productivity to increase at Sites U1345 and U1343. However, at Bowers Ridge Site U1341, productivity declined at this time. The pattern of primary productivity across the Bering Sea underscores that understanding the myriad drivers of primary productivity is essential as we prepared for decreased sea ice in the future.

Data used in this manuscript are archived at the National Center for Environmental Information (https://www.ncdc.noaa.gov/paleo/study/20326).

Acknowledgements

The authors thank the captain and crew of the JOIDES Resolution and Exp. 323 co-chief scientists Christina Ravelo and Kozo Takahashi. We acknowledge the two reviewers, Thomas Cronin and Jason Addison who provided us with thoughtful comments that greatly improved this manuscript. This work was partially supported by National Science Foundation, Office of Polar Programs Arctic Natural Sciences Award #1023537 and a Post Expedition Award from the Consortium for Ocean Leadership.

References

Aizawa, C., Tanimoto, M., and Jordan, R. W.: Living diatom assemblages from North Pacific and Bering Sea surface waters during summer 1999, Deep-Sea Research Part Ii-Topical Studies in Oceanography, 52, 2186-2205, 2005.

Alexander, V. and Chapman, T.: The role of epontic algal communities in Bering Sea ice. In: The Eastern Bering Sea Shelf: Oceanography and Resources, Hood, D. W. and Calder, J. A. (Eds.), University of Washington Press, Seattle, Washington, 1981.

Asahi, H., Kender, S., Ikehara, M., Sakamoto, T., Takahashi, K., Ravelo, A. C., Alvarez Zarikian, C. A., Khim, B. K., and Leng, M. J.: Orbital-scale benthic foraminiferal oxygen isotope stratigraphy at the northern Bering Sea Slope Site U1343 (IODP Expedition 323) and its Pleistocene paleoceanographic significance, Deep Sea Research Part II: Topical Studies in Oceanography, 125–126, 66-83, 2016.

Barr, I. D. and Clark, C. D.: Distribution and pattern of moraines in Far NE Russia reveal former glacial extent, Journal of Maps, 5, 186-193, 2009.

Barron, J. A., Bukry, D., Dean, W. E., Addison, J. A., and Finney, B.: Paleoceanography of the Gulf of Alaska during the past 15,000 years: results from diatoms, silicoflagellates, and geochemistry, Marine Micropaleontology, 72, 176-195, 2009.

Bauch, H. A., Erlenkeuse, H., Helmke, J. P., and Struck, U.: A paleoclimatic evaluatioun of marine oxygen isotope stage 11 in thehigh-northern Atlantic (Nordic seas), Global and Planetary Change, 24, 27-39, 2000.

Berger, A., Crucifix, M., Hodell, D. A., Mangili, C., McManus, J. F., Otto-Bliesner, B., Pol, K., Raynaud, D., Skinner, L. C., Tzedakis, P. C., Wolff, E. W., Yin, Q. Z., Abe-Ouchi, A., Barbante, C., Brovkin, V., Cacho, I., Capron, E., Ferretti, P., Ganopolski, A., Grimalt, J. O., Hönisch, B., Kawamura, K., Landais, A., Margari, V., Martrat, B., Masson-Delmotte, V., Mokeddem, Z., Parrenin, F., Prokopenko, A. A., Rashid, H.,

Schulz, M., and Vazquez Riveiros, N.: “Interglacials of the last 800,000 years”, Rev Geophys, doi: 10.1002/2015RG000482, 2015. n/a-n/a, 2015.

Berger, A. and Loutre, M. F.: Insolation Values for the Climate of the Last 10 Million Years, Quaternary Science Reviews, 10, 297-317, 1991.

Bertrand, P., Pedersen, T. F., Martinez, P., Calvert, S., and Shimmield, G.: Sea level impact on nutrient cycling in coastal upwelling areas during deglaciation: evidence from nitrogen isotopes, Global Biogeochemical Cycles, 14, 341-355, 2000.

Bowen, D. Q.: Sea level ~400 000 years ago (MIS 11): analogue for present and future sea-level?, Clim Past, 6, 19-29, 2010.

Brigham-Grette, J., Hopkins, D. M., Ivanov, V. F., Basilyan, A. E., Benson, S. L., Heiser, P. A., and Pushkar, V. S.: Last interglacial (isotope stage 5) glacial and sea-level history of coastal Chukotka Peninsula and St. Lawrence Island, Western Beringia, Quaternary Science Reviews, 20, 419-436, 2001.

Brunelle, B. G., Sigman, D. M., Cook, M. S., Keigwin, L., Haug, G. H., Plessen, B., Schettler, G., and Jaccard, S. L.: Evidence from diatom-bound nitrogen isotopes for subarctic Pacific stratification during the last ice age and a link to North Pacific denitrification changes, Paleoceanography, 22, 2007.

Caissie, B. E.: Diatoms as recorders of sea ice in the Bering and Chukchi seas: proxy development and application, PhD, Geosciences, University of Massachusetts Amherst, Amherst, MA, 190 pp., 2012.

Caissie, B. E., Brigham-Grette, J., Lawrence, K. T., Herbert, T. D., and Cook, M. S.: Last Glacial Maximum to Holocene sea surface conditions at Umnak Plateau, Bering Sea, as inferred from diatom, alkenone, and stable isotope records, Paleoceanography, 25, 10.1029/2008pa001671, 2010.

880 Candy, I., Schreve, D. C., Sherriff, J., and Tye, G. J.: Marine Isotope Stage 11:
881 Palaeoclimates, palaeoenvironments and its role as an analogue for the current
882 interglacial, Earth-Science Reviews, 128, 18-51, 2014.

883 Cavalieri, D. J., Parkinson, P., Gloersen, P., and Zwally: Sea Ice Concentrations from
884 Nimbus-7 SMMR and DMSP SSM/I Passive Microwave Data, 1996-2008. National
885 Snow and Ice Data Center, Boulder, CO, 1996.

886 Chaisson, W. P., Poli, M. S., and Thunell, R. C.: Gulf Stream and Western Boundary
887 Undercurrent variations during MIS 10 -12 at Site 1056, Blake-Bahama Outer Ridge,
888 Marine Geology, 189, 79-105, 2002.

889 Cook, M. S., Ravelo, A. C., Mix, A., Nesbitt, I. M., and Miller, N. V.: Tracing subarctic
890 Pacific water masses with benthic foraminiferal stable isotopes during the LGM and late
891 Pleistocene, Deep Sea Research Part II: Topical Studies in Oceanography, 125–126, 84-
892 95, 2016.

893 Cooper, L. W., Whitledge, T. E., Grebmeier, J. M., and Wieingartner, T.: The nutrient,
894 salinity, and stable oxygen isotope composition of Bering and Chukchi Seas waters in
895 and near the Bering Strait, Journal of Geophysical Research, 102, 12563-12573, 1997.

896 Cronin, T. M., Polyak, L., Reed, D., Kandiano, E. S., Marzen, R. E., and Council, E. A.:
897 A 600-ka Arctic sea-ice record from Mendeleev Ridge based on ostracodes, Quaternary
898 Science Reviews, 79, 157-167, 2013.

899 D'Anjou, R. M., Wei, J. H., Casteneda, I. S., Brigham-Grette, J., Petsch, S. T., and
900 Finkelstein, D. B.: High-latitude environmental change during MIS 9 and 11:
901 biogeochemical evidence from Lake El'gygytgyn, Far East Russia, Clim Past, 9, 567-581,
902 2013.

903 de Vernal, A. and Hillaire-Marcel, C.: Natural variability of Greenland climate,
904 vegetation, and ice volume during the past million years, Science, 320, 1622-1625, 2008.

905 DeBoer, A. M. and Nof, D.: The Exhaust Valve of the North Atlantic, Journal of Climate,
906 17, 417-422, 2004.

907 Dickson, A. J., Beer, C. J., Dempsey, C., Maslin, M. A., Bendle, J. A., McClymont, E. L.,
908 and Pancost, R. D.: Oceanic forcing of the Marine Isotope Stage 11 interglacial, Nature
909 Geoscience, 2, 428-433, 2009.

910 Droxler, A. W., Alley, R. B., Howard, W. R., Poore, R. Z., and Burckle, L. H.: Unique
911 and exceptionally long interglacial Marine Isotope Stage 11: window into Earth's warm
912 future climate. In: Earth's Climate and Orbital Eccentricity: The Marine Isotope Stage 11
913 Question, Droxler, A. W., Poore, R. Z., and Burckle, L. H. (Eds.), American Geophysical
914 Union, Washington, DC, 2003.

915 Dutton, A., Carlson, A. E., Long, A. J., Milne, G. A., Clark, P. U., DeConto, R., Horton,
916 B. P., Rahmstorf, S., and Raymo, M. E.: Sea-level rise due to polar ice-sheet mass loss
917 during past warm periods, Science, 349, 2015.

918 Eberl, D. D.: User's Guide to RockJock--a Program for Determining Quantitative
919 Mineralogy from Powder X-Ray Diffraction Data, US Geological Survey, Open-File
920 Report 03-78, Boulder, CO, 2003.

921 EPICA Community Members: Eight glacial cycles from an Antarctic ice core, Nature,
922 429, 623-628, 2004.

923 Flores, J. A., Gersonde, R., and Sierro, F. J.: Pleistocene fluctuations in the Agulhas
924 Current Retroflection based on the calcareous plankton record, Marine
925 Micropaleontology, 37, 1-22, 1999.

926 Flores, J. A. and Sierro, F. J.: Revised technique for calculation of calcareous nannofossil
927 accumulation rates, Micropaleontology, 43, 321-324, 1997.

928 Fryxell, G. A. and Hasle, G. R.: *Thalassiosira eccentrica* (Ehreb.) Cleve, *T. symmetrica*
929 sp. nov., and some related centric diatoms, Journal of Phycology, 8, 297-317, 1972.

930 Glushkova, O. Y.: Geomorphological correlation of Late Pleistocene glacial complexes
931 of Western and Eastern Beringia, Quaternary Science Reviews, 20, 405-417, 2001.

932 Gualtieri, L. and Brigham-Grette, J.: The age and origin of the Little Diomede Island
933 upland surface, Arctic, 54, 12-21, 2001.

934 Gualtieri, L., Glushkova, O., and Brigham-Grette, J.: Evidence for restricted ice extent
935 during the last glacial maximum in the Koryak Mountains of Chukotka, far eastern
936 Russia, Geological Society of America Bulletin, 112, 1106-1118, 2000.

937 Håkansson, H.: A compilation and evaluation of species in the general *Stephanodiscus,*
938 *Cyclostephanos,* and *Cyclotella* with a new genus in the family Stephanodiscaceae,
939 Diatom Research, 17, 1-139, 2002.

940 Hall, I. R., McCave, L. N., Shackleton, N. J., Weedon, G. P., and Harris, S. E.:
941 Intensified deep Pacific inflow and ventilation in Pleistocene glacial times, Nature, 412,
942 809-812, 2001.

943 Hasle, G. R. and Heimdal, B. R.: Morphology and distribution of the marine centric
944 diatom *Thalassiosira antarctica* Comber, Journal of the Royal Microscopical Society, 88,
945 357-369, 1968.

946 Hay, M. B., Dallimore, A., Thomson, R. E., Calvert, S. E., and Pienitz, R.: Siliceous
947 microfossil record of late Holocene oceanography and climate along the west coast of
948 Vancouver Island, British Columbia (Canada), Quaternary Research, 67, 33-49, 2007.

949 Heiser, P. A. and Roush, J. J.: Pleistocene glaciations in Chukotka, Russia: moraine
950 mapping using satellite synthetic aperture radar (SAR) imagery, Quaternary Science
951 Reviews, 20, 393-404, 2001.

952 Hopkins, D. M.: Cenozoic Hhistory of the Bering Land Bridge, Science, 129, 1519-1528,
953 1959.

954 Hopkins, D. M.: The paleogeography and climatic history of Beringia during late
955 Cenozoic Time, Internord, 12, 121-150, 1972.

956 Hopkins, D. M.: Pleistocene glaciation on St. George, Pribilof Islands, Science, 1966.
957 343-345, 1966.

958 Horner, R.: Sea Ice Biota, CRC Press, Inc, Boca Raton, FL, 1985.

959 Hu, A. X., Meehl, G. A., Otto-Bliesner, B. L., Waelbroeck, C., Han, W. Q., Loutre, M.
960 F., Lambeck, K., Mitrovica, J. X., and Rosenbloom, N.: Influence of Bering Strait flow
961 and North Atlantic circulation on glacial sea-level changes, Nature Geoscience, 3, 118-
962 121, 2010.

963 Huston, M. M., Brigham-Grette, J., and Hopkins, D. M.: Paleogeographic significance of
964 middle Pleistocene glaciomarine deposits on Baldwin Peninsula, northwestern Alaska,
965 Annals of Glaciology, 14, 111-114, 1990.

966 IPCC: Climate Change 2013: The Physical Science Basis. Contribution of Working
967 Group I to the Fifth Assessment Report of the Intergovernmental Panel on Climate
968 Change. Stocker, T. F., Qin, D., Plattner, G.-K., Tignor, M., Allen, S. K., Boschung, J.,
969 Nauels, A., Xia, Y., Bex, V., and Midgley, P. M. (Eds.), Cambridge University Press,
970 Cambidge, U.K. and New York, NY, USA, 2013.

971 Iwasaki, S., Takahashi, K., Kanematsu, Y., Asahi, H., Onodera, J., and Ravelo, A. C.:
972 Paleoproductivity and paleoceanography of the last 4.3 Myrs at IODP Expedition 323
973 Site U1341 in the Bering Sea based on biogenic opal content, Deep Sea Research Part II:
974 Topical Studies in Oceanography, 125–126, 145-154, 2016.

975 Kandiano, E. S., Bauch, H. A., Fahl, K., Helmke, J. P., Roehl, U., Perez-Folgado, M., and
976 Cacho, I.: The meridional temperature gradient in the eastern North Atlantic during MIS
977 11 and its link to the ocean-atmosphere system, Palaeogeography Palaeoclimatology
978 Palaeoecology, 333, 24-39, 2012.

979 Kanematsu, Y., Takahashi, K., Kim, S., Asahi, H., and Khim, B.-K.: Changes in biogenic
980 opal productivity with Milankovitch cycles during the last 1.3 Ma at IODP Expedition
981 323 Sites U1341, U1343, and U1345 in the Bering Sea, Quaternary International, 310,
982 213-220, 2013.

983 Kariya, C., Hyodo, M., Tanigawa, K., and Sato, H.: Sea-level variation during MIS 11
984 constrained by stepwise Osaka Bay extensions and its relation with climatic evolution,
985 Quaternary Science Reviews, 29, 1863-1879, 2010.

986 Kato, Y., Onodera, J., Suto, I., Teraishi, A., and Takahashi, K.: Pliocene and Pleistocene
987 paleoceanography in the western subarctic Pacific based on diatom analyses of ODP Leg
988 145 Hole 884B and IODP Expedition 323 Holes U1341B and U1343E, Deep Sea
989 Research Part II: Topical Studies in Oceanography, 125–126, 29-37, 2016.

990 Katsuki, K. and Takahashi, K.: Diatoms as paleoenvironmental proxies for seasonal
991 productivity, sea-ice and surface circulation in the Bering Sea during the late Quaternary,
992 Deep Sea Research II, 52, 2110-2130, 2005.

993 Kaufman, D., Young, N. E., Briner, J. P., and Manley, W. F.: Alaska Palaeo-Glacier
994 Atlas (Version 2). In: Developments in Quaternary Science, Ehlers, J., Gibbard, P. L.,
995 and Hughes, P. D. (Eds.), Amsterdam, The Netherlands, 2011.

996 Kaufman, D. S.: Aminostratigraphy of Pliocene-Pleistocene high-sea-level deposits,
997 Nome coastal plain and adjacent nearshore area, Alaska, Geological Society of America
998 Bulletin, 104, 40-52, 1992.

999 Kaufman, D. S. and Brigham-Grette, J.: Aminostratigraphic correlations and
1000 paleotemperature implications, Pliocene-Pleistocene high sea-level deposits,
1001 Northwestern Alaska, Quaternary Science Reviews, 12, 21-33, 1993.

1002 Kaufman, D. S., Manley, W. F., Forman, S. L., and Layer, P. W.: Pre-Late-Wisconsin
1003 glacial history, coastal Ahklun Mountains, southwestern Alaska - new amino acid,
1004 thermoluminescence, and $^{40}Ar/^{39}Ar$ results, Quaternary Science Reviews, 20, 337-352,
1005 2001.

1006 Kaufman, D. S., Walter, R. C., Brigham-Grette, J., and Hopkins, D. M.: Middle
1007 Pleistocene age of the Nome River glaciation, northwestern Alaska, Quaternary
1008 Research, 36, 277-293, 1991.

1009 Keigwin, L. D., Donnelly, J. P., Cook, M. S., Driscoll, N. W., and Brigham-Grette, J.:
1010 Rapid sea-level rise and Holocene climate in the Chukchi Sea, Geology, 34, 861-864,
1011 2006.

1012 Kim, S., Khim, B.-K., and Takahashi, K.: Late Pliocene to early Pleistocene (2.4–1.25
1013 Ma) paleoproductivity changes in the Bering Sea: IODP expedition 323 Hole U1343E,
1014 Deep Sea Research Part II: Topical Studies in Oceanography, 125–126, 155-162, 2016.

1015 Kim, S., Khim, B. K., and Goo Cho, H.: Clay mineral stratigraphy during the last 2.4 Ma
1016 at IODP Exp. 323 Site U1343 in the Bering Sea, Marine Geology, 359, 163-168, 2015.

1017 Kindler, P. and Hearty, P. J.: Elevated marine terraces from Eleuthera (Bahamas) and
1018 Bermuda: sedimentological, petrographic, and geochronological evidence for important
1019 deglaciation events during the middle Pleistocene, Global and Planetary Change, 24, 41-
1020 58, 2000.

1021 Kleinen, T., Hildebrandt, S., Prange, M., Rachmayani, R., Mueller, S., Bezrukova, E.,
1022 Brovkin, V., and Tarasov, P. E.: The climate and vegetation of Marine Isotope Stage 11-

Model results and proxy-based reconstructions at global and regional scale, Quaternary International, 348, 247-265, 2014.

Knudson, K. P. and Ravelo, A. C.: North Pacific Intermediate Water circulation enhanced by the closure of the Bering Strait, Paleoceanography, 30, 1287-1304, 2015.

Koizumi, I.: The Late Cenozoic diatoms of Sites 183-193, Leg 19 Deep Sea Drilling Project, Initial Reports of the Deep Sea Drilling Project, 19, 805-855, 1973.

Kowalik, Z.: Bering Sea Tides. In: Dynamics of the Bering Sea, Loughlin, T. R. and Ohtani, K. (Eds.), Universtiy of Alaska Sea Grant, Fairbanks, AK, 1999.

Lisiecki, L. E. and Raymo, M. E.: A Pliocene-Pleistocene stack of 57 globally distributed benthic delta O-18 records, Paleoceanography, 20, 10.1029/2004PA001071, 2005.

Liu, Z. H., Altabet, M. A., and Herbert, T. D.: Glacial-interglacial modulation of eastern tropical North Pacific denitrification over the last 1.8-Myr, Geophysical Research Letters, 32, 2005.

Lopes, C., Mix, A. C., and Abrantes, F.: Diatoms in northeast Pacific surface sediments as paleoceanographic proxies, Marine Micropaleontology, 60, 45-65, 2006.

Loutre, M. F. and Berger, A.: Marine Isotope Stage 11 as an analogue for the present interglacial, Global and Planetary Change, 36, 209-217, 2003.

Lozhkin, A. V. and Anderson, P.: Vegetation responses to interglacial warming in the Arctic: examples from Lake El'gygytgyn, Far East Russian Arctic, Clim Past, 9, 1211-1219, 2013.

Lundholm, N. and Hasle, G. R.: Are *Fragilariopsis cylindrus* and *Fragilariopsis nana* bipolar diatoms? Morphological and molecular analyses of two sympatric species, Nova Hedwigia, 133, 231-250, 2008.

1046 Lundholm, N. and Hasle, G. R.: *Fragilariopsis* (Bacillariophyceae) of the Northern
1047 Hemisphere--morphology, taxonomy, phylogeny and distribution, with a description of
1048 *F. pacifica* sp. nov., Phycologia, 49, 438-460, 2010.

1049 Lyle, M., Heusser, L., Herbert, T., Mix, A. C., and Barron, J.: Interglacial theme and
1050 variations: 500 k.y. of orbital forcing and associated responses from the terrestrial and
1051 marine biosphere, U.S. Pacific Northwest, Geology, 29, 1115-1118, 2001.

1052 Manley, W. F.: Digital Elevation Model (DEM) for the Bering Land Bridge, INSTAAR,
1053 University of Colorado, Boulder, CO, 2002.

1054 Maurer, B. A. and McGill, B. J.: Chapter 5: measurement of species diversity. In:
1055 Biological Diversity, Magurran, A. E. and McGill, B. J. (Eds.), Oxford University Press,
1056 New York, 2011.

1057 McKay, R., Naish, T., Powell, R., Barrett, P., Scherer, R., Talarico, F., Kyle, P., Monien,
1058 D., Kuhn, G., Jackolski, C., and Williams, T.: Pleistocene variability of Antarctic Ice
1059 Sheet extent in the Ross Embayment, Quaternary Science Reviews, 34, 93-112, 2012.

1060 McManus, J., Oppo, D. W., Cullen, J. L., and Healey, S.: Marine Isotope Stage 11 (MIS
1061 11): analog for Holocene and future climate. In: Earth's Climate and Orbital Eccentricity:
1062 The Marine Isotope Stage 11, Droxler, A. W., Poore, R. Z., and Burkle, L. H. (Eds.),
1063 Geophysical Monograph 137, American Geophysical Union, Washington, DC, 2003.

1064 McQuoid, M. R. and Hobson, L. A.: A Holocene record of diatom and silicoflagellate
1065 microfossils in sediments of Saanich Inlet, ODP Leg 169S, Marine Geology, 174, 111-
1066 123, 2001.

1067 Medlin, L. K. and Hasle, G. R.: Some *Nitzschia* and related diatom species from fast ice
1068 samples in the Arctic and Antarctic, Polar Biology, 10, 451-479, 1990.

1069 Medlin, L. K. and Priddle, J.: Polar Marine Diatoms, British Antarctic Survey, Natural
1070 Environment Research Council, Cambridge, 1990.

1071 Melles, M., Brigham-Grette, J., Minyuk, P., Nowaczyk, N. R., Wennrich, V., DeConto,
1072 R. M., Anderson, P. M., Andreev, A. A., Coletti, A., Cook, T. L., Haltia-Hovi, E.,
1073 Kukkonen, M., Lozhkin, A. V., Rosen, P., Tarasov, P. E., Vogel, H., and Wagner, B.: 2.8
1074 Million years of Arctic climate change from Lake El'gygytgyn, NE Russia, Science,
1075 2012. 2012.

1076 Meyers, P. A.: Preservation of elemental and isotopic source identification of
1077 sedimentary organic matter, Chemical Geology, 114, 289-302, 1994.

1078 Milker, Y., Rachmayani, R., Weinkauf, M. F. G., Prange, M., Raitzsch, M., Schulz, M.,
1079 and Kucera, M.: Global and regional sea surface temperature trends during Marine
1080 Isotope Stage 11, Clim Past, 9, 2231-2252, 2013.

1081 Miller, G. H., Brigham-Grette, J., Anderson, L., Bauch, H. A., Douglas, M. A., Edwards,
1082 M. E., Elias, S. A., Finney, B. P., Funder, S., Herbert, T., Hinzman, L. D., Kaufman, D.
1083 K., MacDonald, G. M., Robock, A., Serreze, M. C., Smol, J. P., Spielhagen, R. F., Wolfe,
1084 A. P., and Wolff, E. W.: Temperature and precipitation history of the Arctic. In: Past
1085 Climate Variability and Change in the Arctic and at High Latitudes, Research, U. S. C. C.
1086 P. a. S. o. G. C. (Ed.), U.S. Geological Survey, Reston, VA, 2009.

1087 Miller, G. H. and De Vernal, A.: Will greenhouse warming lead to Northern Hemisphere
1088 ice-sheet growth?, Nature, 355, 244-246, 1992.

1089 Muller, P. J.: C-N Ratios in Pacific Deep-Sea Sediments - Effect of Inorganic
1090 Ammonium and Organic Nitrogen Compounds Sorbed by Clays, Geochimica Et
1091 Cosmochimica Acta, 41, 765-776, 1977.

1092 Naish, T., Powell, R., Levy, R., Wilson, G., Scherer, R., Talarico, F., Krissek, L.,
1093 Niessen, F., Pompilio, M., Wilson, T., Carter, L., DeConto, R., Huybers, P., McKay, R.,

Pollard, D., Ross, J., Winter, D., Barrett, P., Browne, G., Cody, R., Cowan, E., Crampton, J., Dunbar, G., Dunbar, N., Florindo, F., Gebhardt, C., Graham, I., Hannah, M., Hansaraj, D., Harwood, D., Helling, D., Henrys, S., Hinnov, L., Kuhn, G., Kyle, P., Laufer, A., Maffioli, P., Magens, D., Mandernack, K., McIntosh, W., Millan, C., Morin, R., Ohneiser, C., Paulsen, T., Persico, D., Raine, I., Reed, J., Riesselman, C., Sagnotti, L., Schmitt, D., Sjunneskog, C., Strong, P., Taviani, M., Vogel, S., Wilch, T., and Williams, T.: Obliquity-paced Pliocene West Antarctic ice sheet oscillations, Nature, 458, 322-U384, 2009.

Normack, W. R. and Carlson, P. R.: Giant submarine canyons: is size any clue to their importance in the rock record? In: Geological Society of America Special Paper, Chan, M. A. and Archer, A. W. (Eds.), Geological Society of America, Boulder, CO, 2003.

Nürnberg, D., Wollenburg, I., Dethleff, D., Eicken, H., Kassens, H., Letzig, T., Reimnitz, E., and Thiede, J.: Sediments in Arctic Sea-Ice - Implications for Entrainment, Transport and Release, Marine Geology, 119, 185-214, 1994.

Onodera, J. and Takahashi, K.: Diatoms and siliceous flagellates (silicoflagellates, ebridians, and endoskeletal dinoflagellate *Actiniscus*) from the Subarctic Pacific, Memoirs of the Faculty of Sciences Kyushu University., Series D, Earth and Planetary Sciences, 31, 105-136, 2007.

Onodera, J., Takahashi, K., and Nagatomo, R.: Diatoms, silicoflagellates, and ebridians at Site U1341 on the western slope of Bowers Ridge, IODP Expedition 323, Deep Sea Research Part II: Topical Studies in Oceanography, 125–126, 8-17, 2016.

Ortiz, J. D., Nof, D., Polyak, L., St-Onge, G., Lisé-Pronovost, A., Naidu, S., Darby, D., and Brachfeld, S.: The Late Quaternary Flow through the Bering Strait Has Been Forced by the Southern Ocean Winds, Journal of Physical Oceanography, 42, 2014-2029, 2012.

PAGES, P. I. W. G. o., Berger, A., Crucifix, M., Hodell, D. A., Mangili, C., McManus, J. F., Otto-Bliesner, B., Pol, K., Raynaud, D., Skinner, L. C., Tzedakis, P. C., Wolff, E. W.,

1120 Yin, Q. Z., Abe-Ouchi, A., Barbante, C., Brovkin, V., Cacho, I., Capron, E., Ferretti, P.,
1121 Ganopolski, A., Grimalt, J. O., Hoenisch, B., Kawamura, K., Landais, A., Margari, V.,
1122 Martrat, B., Masson-Delmotte, V., Mokeddem, Z., Parrenin, F., Prokopenko, A. A.,
1123 Rashid, H., Schulz, M., and Riveiros, N. V.: Interglacials of the last 800,000years, Rev
1124 Geophys, 54, 162-219, 2016.

1125 Perdue, E. M. and Koprivnjak, J.-F.: Using the C/N ratio to estimate terrigenous inputs of
1126 organic matter to aquatic environments, Estuar Coast Shelf S, 73, 65-72, 2007.

1127 Pol, K.: Links between MIS 11 millennial to sub-millennial climate variability and long
1128 term trends as revealed by new high resolution EPICA Dome C deuterium data - A
1129 comparison with the Holocene, Clim Past, 7, 437-450, 2011.

1130 Poli, M. S., Meyers, P. A., and Thunell, R. C.: The western North Atlantic record of MIS
1131 13 to 10: Changes in primary productivity, organic carbon accumulation and benthic
1132 foraminiferal assemblages in sediments from the Blake Outer Ridge (ODP Site 1058),
1133 Palaeogeography, Palaeoclimatology, Palaeoecology, 295, 89-101, 2010.

1134 Pollard, D. and DeConto, R. M.: Modelling West Antarctic ice sheet growth and collapse
1135 through the past five million years, Nature, 458, 329-U389, 2009.

1136 Prokopenko, A. A., Bezrukova, E. V., Khursevich, G. K., Solotchina, E. P., Kuzmin, M.
1137 I., and Tarasov, P. E.: Climate in continental interior Asia during the longest interglacial
1138 of the past 500 000 years: the new MIS 11 records from Lake Baikal, SE Siberia, Clim
1139 Past, 6, 31-48, 2010.

1140 Pushkar, V. S., Roof, S. R., Cherepanova, M. V., Hopkins, D. M., and Brigham-Grette,
1141 J.: Paleogeographic and paleoclimatic significance of diatoms from Middle Pleistocene
1142 marine and glaciomarine deposits on Baldwin Peninsula, northwestern Alaska,
1143 Palaeogeography, Palaeoclimatology, Palaeoecology, 152, 67-85, 1999.

1144 Raymo, M. E. and Mitrovica, J. X.: Collapse of polar ice sheets during the stage 11
1145 interglacial, Nature, 483, 453-456, 2012.

1146 Raymo, M. E., Mitrovica, J. X., O'Leary, M. J., DeConto, R. M., and Hearty, P. J.:
1147 Departures from eustasy in Pliocene sea-level records, Nature Geoscience, 4, 328-332,
1148 2011.

1149 Raynaud, D., Barnola, J. M., Souchez, R., Lorrain, R., Petit, J. R., Duval, P., and
1150 Lipenkov, V. Y.: The record for Marine Isotopic Stage 11, Nature, 436, 39-40, 2005.

1151 Redfield, A. C., Ketchum, B. H., and Richards, F. A.: The inuence of organisms on the
1152 composition of sea water. In: The Sea, Hill, M. N. (Ed.), Wiley, New ork, 1963.

1153 Reimnitz, E., McCormick, M., Bischof, J., and Darby, D. A.: Comparing sea-ice
1154 sediment load with Beaufort Sea shelf deposits: is entrainment selective?, Journal of
1155 Sedimentary Research, 68, 777-787, 1998.

1156 Reyes, A. V., Carlson, A. E., Beard, B. L., Hatfield, R. G., Stoner, J. S., Winsor, K.,
1157 Welke, B., and Ullman, D. J.: South Greenland ice-sheet collapse during Marine Isotope
1158 Stage 11, Nature, 510, 525-+, 2014.

1159 Rohling, E. J., Braun, K., Grant, K., Kucera, M., Roberts, A. P., Siddall, M., and
1160 Trommer, G.: Comparison between Holocene and Marine Isotope Stage-11 sea-level
1161 histories, Earth and Planetary Science Letters, 291, 97-105, 2010.

1162 Rohling, E. J., Foster, G. L., Grant, K. M., Marino, G., Roberts, A. P., Tamisiea, M. E.,
1163 and Williams, F.: Sea-level and deep-sea-temperature variability over the past 5.3 million
1164 years (vol 508, pg 477, 2014), Nature, 510, 432-432, 2014.

1165 Saito, K. and Taniguchi, A.: Phytoplankton communities in the Bering Sea and adjacent
1166 seas II: spring and summer communities in seasonally ice-covered areas, Astarte, 11, 27-
1167 35, 1978.

1168 Sancetta, C. A.: Distribution of diatom species in surface sediments of the Bering and
1169 Okhotsk seas, Micropaleontology, 28, 221-257, 1982.

1170 Sancetta, C. A.: Oceanographic and ecologic significance of diatoms in surface sediments
1171 of the Bering and Okhotsk seas, Deep Sea Research, 28A, 789-817, 1981.

1172 Sancetta, C. A.: Three species of *Coscinodiscus* Ehrenberg from North Pacific sediments
1173 examined in the light and scanning electron microscopes, Micropaleontology, 33, 230-
1174 241, 1987.

1175 Sancetta, C. A. and Robinson, S. W.: Diatom evidence on Wisconsin and Holocene
1176 events in the Bering Sea, Quaternary Research, 20, 232-245, 1983.

1177 Sancetta, C. A. and Silvestri, S. M.: Pliocene-Pleistocene evolution of the North Pacific
1178 ocean-atmosphere system, interpreted from fossil diatoms, Paleoceanography, 1, 163-
1179 180, 1986.

1180 Schandelmeier, L. and Alexander, V.: An analysis of the influence of ice on spring
1181 phytoplankton population structure in the southeast Bering Sea, Limnology and
1182 Oceanography, 26, 935-943, 1981.

1183 Scherer, R. P.: A new method for the determination of absolute abundance of diatoms
1184 and other silt-sized sedimentary particles, Journal of Paleolimnology, 12, 171-179, 1994.

1185 Scherer, R. P., Aldahan, A., Tulaczyk, S., Possnert, G., Engelhardt, H., and Kamb, B.:
1186 Pleistocene collapse of the West Antarctic Ice Sheet, Science, 281, 82-85, 1998.

1187 Schlung, S. A., Ravelo, A. C., Aiello, I. W., Andreasen, D. H., Cook, M. S., Drake, M.,
1188 Dyez, K. A., Guilderson, T. P., LaRiviere, J. P., Stroynowski, Z., and Takahashi, K.:
1189 Millennial-scale climate change and intermediate water circulation in the Bering Sea
1190 from 90 ka: A high-resolution record from IODP Site U1340, Paleoceanography, 28,
1191 2013.

1192 Schrader, H. J. and Gersonde, R.: Diatoms and silicoflagellates. In: Micropaleontological
1193 counting methods and techniques - an exercise on an eight metres section of the Lower
1194 Pliocene of Capo Rossello, Sicily, Zachariasse, W. J., Riedel, W. R., Sanfilippo, A.,
1195 Schmidt, R. R., Brolsma, M. J., Schrader, H. J., Gersonde, R., Drooger, M. M., and
1196 Broekman, J. A. (Eds.), Utrecht Micropaleontological Bulletin, Netherlands, 1978.

1197 Schubert, C. J. and Calvert, S. E.: Nitrogen and carbon isotopic composition of marine
1198 and terrestrial organic matter in Arctic Ocean sediments: implications for nutrient
1199 utilization and organic matter composition, Deep Sea Research I, 48, 789-810, 2001.

1200 Schumacher, J. D. and Stabeno, P. J.: Continental shelf of the Bering Sea. In: The sea,
1201 Robinson, A. R. and Brink, K. H. (Eds.), John Wiley and Sons, New York, 1998.

1202 Shiga, K. and Koizumi, I.: Latest Quaternary oceanographic changes in the Okhotsk Sea
1203 based on diatom records, Marine Micropaleontology, 38, 91-117, 2000.

1204 Sigman, D., Altabet, M., Francois, R., McCorkle, D., and Gaillard, J.-F.: The isotopic
1205 composition of diatom-bound nitrogen in Southern Ocean sediments, Paleoceanography,
1206 14, 118-134, 1999.

1207 Smol, J. P.: The paleolimnologist's Rosetta Stone: calibrating indicators to environmental
1208 variables using surface-sediment training sets. In: Pollution of lakes and rivers: a
1209 paleoenvironmental perspective, Smol, J. P. (Ed.), Key issues in environmental change,
1210 Oxford University Press, New York, 2002.

1211 Springer, A. M., McRoy, C. P., and Flint, M. V.: The Bering Sea green belt: shelf edge
1212 processes and ecosystem production, Fisheries Oceanography, 5, 205-223, 1996.

1213 St. John, K.: Cenozoic ice-rafting history of the central Arctic Ocean: Terrigenous sands
1214 on the Lomonosov Ridge, Paleoceanography, 23, 10.1029/2007pa001483, 2008.

1215 Stabeno, P. J., Schumacher, J. D., and Ohtani, K.: The physical oceanography of the
1216 Bering Sea. In: Dynamics of the Bering Sea: a summary of physical, chemical, and
1217 biological characteristics, and a synopsis of research on the Bering Sea, Loughlin, T. R.
1218 and Ohtani, K. (Eds.), University of Alaska Sea Grant, Fairbanks, AK, 1999.

1219 Stroynowski, Z., Ravelo, A. C., and Andreasen, D.: A Pliocene to recent history of the
1220 Bering Sea at Site U1340A, IODP Expedition 323, Paleoceanography, 30, 1641-1656,
1221 2015.

1222 Syvertsen, E. E.: Resting Spore Formation in Clonal Cultures of *Thalassiosira antarctica*
1223 Comber, *T. nordenskioeldii* Cleve and *Detonula confervacea* (Cleve) Gran, Nova
1224 Hedwigia, 64, 41-63, 1979.

1225 Takahashi, K., Ravelo, A. C., Alvarez Zarikian, C. A., and Scientists, E.: Proceedings of
1226 the Integrated Ocean Drilling Program. Tokyo, 2011.

1227 Tarasov, P. E., Nakagawa, T., Demske, D., Österle, H., Igarashi, Y., Kitagawa, J.,
1228 Mokhova, L., Bazarova, V., Okuda, M., Gotanda, K., Miyoshi, N., Fujiki, T., Takemura,
1229 K., Yonenobu, H., and Fleck, A.: Progress in the reconstruction of Quaternary climate
1230 dynamics in the Northwest Pacific: A new modern analogue reference dataset and its
1231 application to the 430-kyr pollen record from Lake Biwa, Earth-Science Reviews, 108,
1232 64-79, 2011.

1233 Teitler, L., Florindo, F., Warnke, D. A., Filippelli, G. M., Kupp, G., and Taylor, B.:
1234 Antarctic Ice Sheet response to a long warm interval across Marine Isotope Stage 31: A
1235 cross-latitudinal study of iceberg-rafted debris, Earth and Planetary Science Letters, 409,
1236 109-119, 2015.

1237 Teraishi, A., Suto, I., Onodera, J., and Takahashi, K.: Diatom, silicoflagellate and
1238 ebridian biostratigraphy and paleoceanography in IODP 323 Hole U1343E at the Bering
1239 slope site, Deep Sea Research Part II: Topical Studies in Oceanography, 125–126, 18-28,
1240 2016.

1241 Ternois, Y., Kawamura, K., Keigwin, L., Ohkouchi, N., and Nakatsuka, T.: A biomarker
1242 approach for assessing marine and terrigenous inputs to the sediments of Sea of Okhotsk
1243 for the last 27,000 years, Geochimica et Cosmochimica Acta, 65, 791-802, 2001.

1244 Tomas, C. R.: Identifying marine diatoms and dinoflagellates, Academic Press, Inc.
1245 Harcourt Brace and Co., Boston, U.S.A., 1996.

1246 Tzedakis, P. C.: The MIS 11 – MIS 1 analogy, southern European vegetation,
1247 atmospheric methane and the "early anthropogenic hypothesis", Clim Past, 6, 131-144,
1248 2010.

1249 van Hengstum, P. J., Scott, D. B., and Javaux, E. J.: Foraminifera in elevated Bermudian
1250 caves provide further evidence for +21m eustatic sea level during Marine Isotope Stage
1251 11, Quaternary Science Reviews, 28, 1850-1860, 2009.

1252 Voelker, A. H. L., Rodrigues, T., Billups, K., Oppo, D., McManus, J., Stein, R., Hefter,
1253 J., and Grimalt, J. O.: Variations in mid-latitude North Atlantic surface water properties
1254 during the mid-Brunhes (MIS 9–14) and their implications for the thermohaline
1255 circulation, Clim Past, 6, 531-552, 2010.

1256 Vogel, H., Meyer-Jacob, C., Melles, M., Brigham-Grette, J., Andreev, A. A., Wennrich,
1257 V., Tarasov, P. E., and Rosen, P.: Detailed insight into Arctic climatic variability during
1258 MIS 11c at Lake El'gygytgyn, NE Russia, Clim Past, 9, 1467-1479, 2013.

1259 von Quillfeldt, C. H.: Identification of some easily confused common diatom species in
1260 Arctic spring blooms, Botanica Marina, 44, 375-389, 2001.

1261 von Quillfeldt, C. H., Ambrose, W. G. J., and Clough, L. M.: High number of diatom
1262 species in first-year ice from the Chukchi Sea, Polar Biology, 26, 806-818, 2003.

1263 Walinsky, S. E., Prahl, F. G., Mix, A. C., Finney, B. P., Jaeger, J. M., and Rosen, G. P.:
1264 Distribution and composition of organic matter in surface sediments of coastal Southeast
1265 Alaska, Continental Shelf Research, 29, 1565-1579, 2009.

1266 Witkowski, A., Lange-Bertalot, H., and Metzeltin, D.: Diatom Flora of Marine Coasts I,
1267 A.R.G. Gantner Verlag K.G., Ruggell, Liechtenstein, 2000.

1268 Young, J. R., Geisen, M., Cros, L., Keleijne, A., Sprengel, C., Probert, I., and
1269 Østengaard, J.: A guide to extant coccolithophore taxonomy, Journal of Nannoplankton
1270 Research, Special Issue, 1, 1-125, 2003.
1271

Table 1: Age-Depth Tie Points Used in the Age Model for U1345

Depth (m CCSF-A)	Age (ka)	Date Type
98.6	337	Foraminifera {Cook, 2016}
115.3	374	Foraminifera {Cook, 2016}
123.2	398.5	Magnetic Susceptibility Correlation
130.6	424	Foraminifera {Cook, 2016}
148.7	478	Foraminifera {Cook, 2016}

Table 2: Depths and Ages of major climate intervals referred to in the text

Interval	Depth begin (m CCSF-A)	Depth end (m CCSF-A)	Begin (ka)	End (ka)
Late MIS 11/10	121.80	110.57	394	364
Beringian Glacial Initiation	124.94	121.80	405	394
Peak MIS 11	130.16	121.80	423	394
Termination V	131.09	130.16	425	423
MIS 12	133.10	131.09	431	425

Table 3: Bering Sea diatom species grouped by environmental niche. In cases where a species appears in more than one niche, the grouping used in this study is highlighted in bold.

Modern Seasonal Succession			
Epontic	**Marginal Ice Zone (MIZ)**	**Both Epontic and MIZ**	**Summer Bloom**
Navicula transitrans	***Bacterosira bathyomphala***	*Actinocyclus curvatulus*	***Coscinodiscus* spp.**
Synedropsis hyperborea	*Chaetoceros furcellatus*	***Fossula arctica***	***Leptocylindrus* sp.**
	Chaetoceros socialis	***Fragilariopsis cylindrus***	***Rhizosolenia* spp.**
	Leptocylindrus sp.	***Fragilariopsis oceanica***	
	Odontella aurita	***Fragilariopsis regina-jahniae***	
	Paralia sulcata	***Navicula pelagica***	
	Porosira glacialis	**Naviculoid pennates**	
	Staurosirella* cf. *pinnata	***Nitzschia* spp.**	
	Thalassionema nitzschioides	***Pinnularia quadratarea***	
	Thalassiosira angulata	***Thalassiosira antarctica* RS**	
	Thalassiosira baltica	***Thalassiosira gravida***	
	Thalassiosira decipiens		
	Thalassiosira hyalina		
	Thalassiosira hyperborea		
	Thalassiosira nordenskioeldii		
	Thalassiosira pacifica		

Continued on next page

Table 3 continued

Water Mass Tracers				*Shelf to Basin Transport*	
Dicothermal	**High Productivity**	**Alaska Stream**	**Warmer Water**	**Neritic**	**Fresh Water**
Actinocyclus curvatulus	***Chaetoceros* spp.**	***Neodenticula seminae***	***Azpeitia tabularis***	***Actinoptychus senarius***	***Lindavia* cf. *ocellata***
Shionodiscus trifultus	***Odontella aurita***		***Stellarimia* stellaris**	***Amphora* sp.**	*Lindavia stylorum*
	Thalassionema nitzschioides		*Thalassionema nitzschioides*	***Lindavia stylorum***	*Staurosirella* cf *pinnata*
	Thalassiosira pacifica		***Thalassiosira eccentrica***	***Delphineis spp.***	***Lindavia radiosa***
	***Thalassiosira* spp. small**		***Shionodiscus oestrupii***	***Detonula confervacea***	
	Thalassiothrix longissima		***Thalassiosira symmetrica***	***Diploneis smithii***	
				Naviculoid pennates	
				Odontella aurita	
				Paralia sulcata	
				Rhaphoneis amphiceros	
				Stephanopyxis turris	
				Thalassiosira angulata	
				Thalassiosira decipiens	
				Thalassiosira eccentrica	

Table 4: Distribution of Laminated Intervals during MIS 11. Note that the depth and age of laminated intervals encompasses all holes drilled, but the median duration is calculated using each of the holes that it is present in.

Lamination	Type	Depth (mbsf)	Age (ka)	Median Duration (kyrs)	Found in Holes
MIS 11.5	II	112.02-111.47	367.23-366.00	0.51	CDE
MIS 11.4	II	113.14-112.94	369.72-369.26	0.34	CD
MIS 11.3	II	114.28-113.95	372.25-371.52	0.73	D
MIS 11.2	II	115.59-114.69	374.75-373.17	1.23	ACE
MIS 11.1	II	121.84-121.18	394.12-392.09	1.10	CE
Termination V	I	130.23-126.51	423.28-410.44	12.04	ACDE

Table 5: Summary Statistics for X-Ray Diffraction

	Mean	Standard	Minimum	Maximum
Full pattern degree of	0.257	0.014	0.242	0.282
Mineral	(wt.	(wt. %)	(wt. %)	(wt. %)
Non-clays				
Quartz	14	2	9	16
Kspar	1	1	0	2
Plag	9	2	5	12
Calcite	Tr	Tr	0	1
Aragonite	2	1	0	3
Dolomite	2	1	1	3
Siderite	1	1	0	2
Amphibole	4	1	3	5
Pyroxene	1	1	0	2
Pyrite	1	0	0	1
Magnetite	Tr	Tr	0	1
Hematite	Tr	Tr	0	1
Goethite	Tr	Tr	0	0
Maghemite	Tr	Tr	0	1
Titanite	1	1	0	3
Tephra	21	5	16	35
Zircon	Tr	Tr	0	0
Total Non-clays	*57*	*2*	*54*	*63*
Clays				
Kaolinite	0	0	0	0
Smectite	0	0	0	0
Illite	8	3	2	11
Biotite	2	1	0	3
Chlorite	33	3	29	38
Muscovite	Tr	1	0	2
Total Clays	*43*	*2*	*37*	*46*
Total	100			

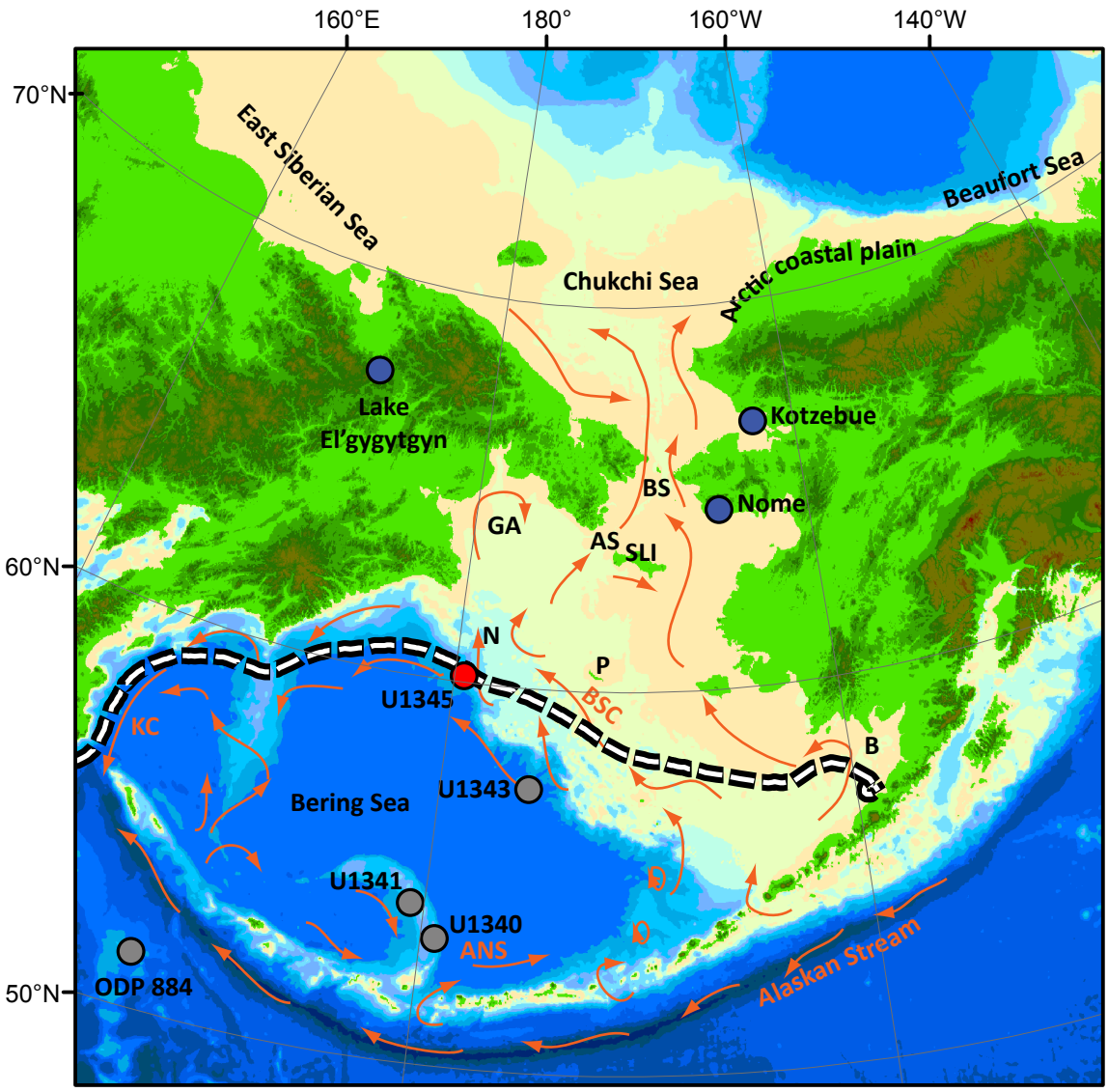

Figure 1. Map of Beringia with locations of cores mentioned in the text (U1345 (red dot), and U1340, U1341, U1343, and ODP Site 884 (grey dots)). Locations of place names from the text are labeled: Aleutian North Slope Current (ANS), Anadyr Strait (AS), Bristol Bay (B), Bering Strait (BS), Bering Slope Current (BSC), Gulf of Anadyr (GA), Kamchatka Current (KC), Navarin Canyon (N), Pribilof Islands (P), St. Lawrence Island (SLI). The white and black dashed line is the maximum extent of sea ice (median over the period 1979-2013) (Cavalieri et al., 1996). Currents are in orange and are modified from Stabeno (1999). Base map is modified from Manley (2002).

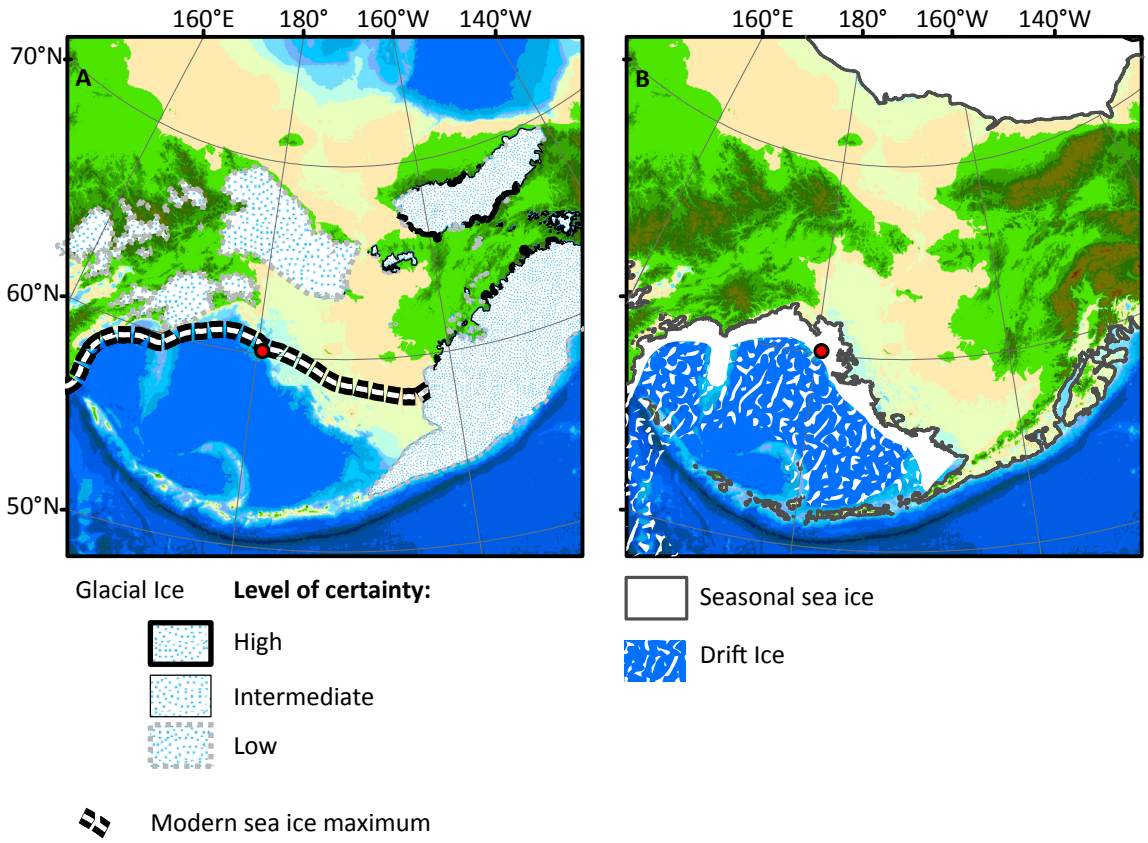

Figure 2. Maximum glacial and sea ice extents in Beringia. **A.** depicts the maximum glacial ice in Beringia as inferred from terminal and lateral moraines (Gualtieri et al., 2000; Heiser and Roush, 2001; Kaufman, et al., 2011; Barr and Clark, 2009). This is not intended to show the maximum extent during a particular glaciation, but rather the maximum possible extent of glacial ice. These moraines are likely from several different major glaciations. The level of certainty is indicated by the thickness of the line at the moraine. The white and black dashed line is the maximum extent of sea ice (median over period 1979-2013) (Cavalieri et al., 1996). **B.** depicts the approximate pattern of sea ice during glacial stages (Katsuki and Takahashi, 2005). The dark grey contour is -140 mapsl, the approximate sea level during MIS 12 (Rohling et al., 2010). Base map is modified from Manley (2002).

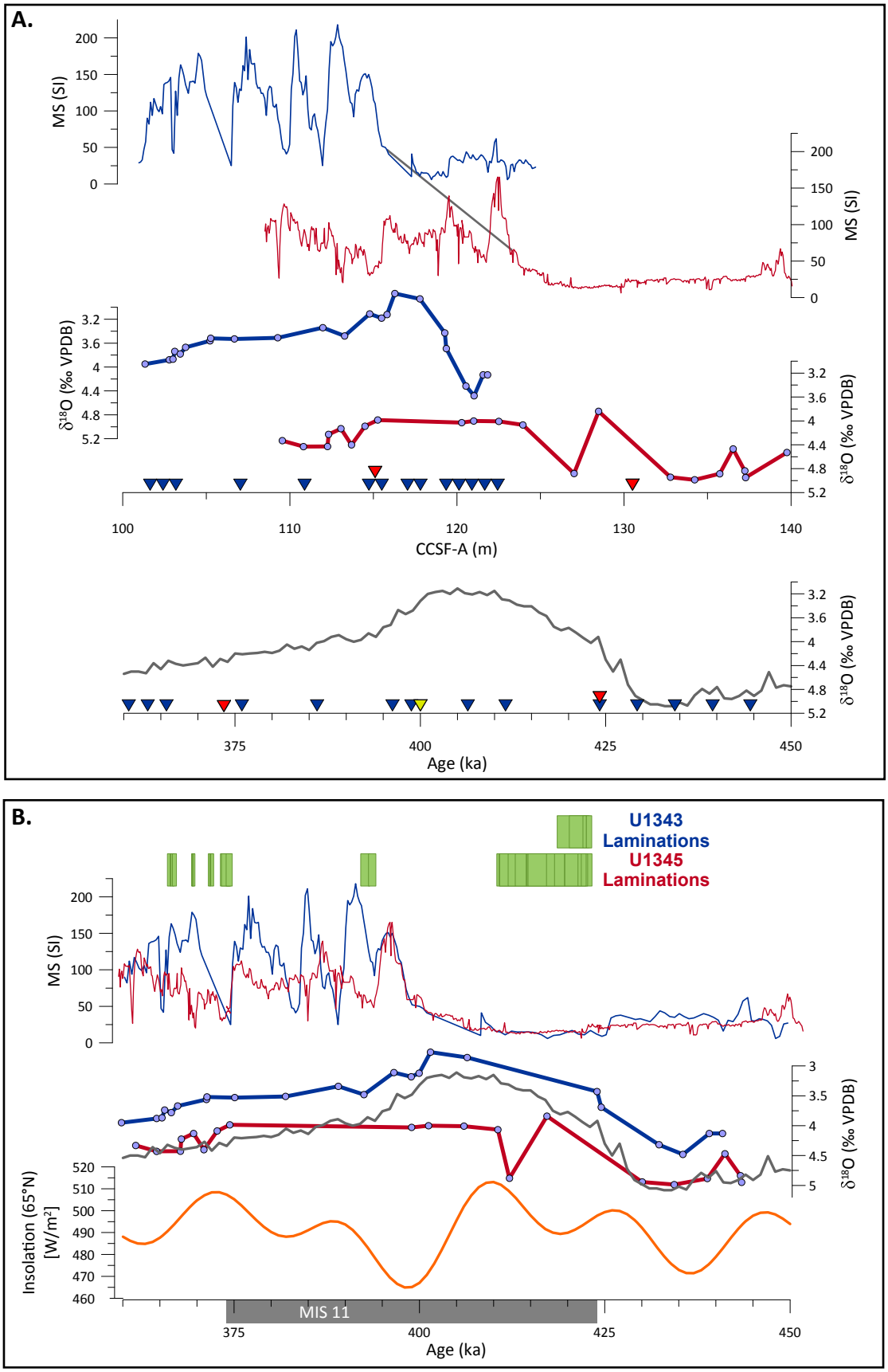
A.
MS (SI)
200
150
100
50
0
δ18O (‰ VPDB)
3.2
3.6
4
4.4
4.8
5.2
100
110
120
130
140
CCSF-A (m)
375
400
425
450
Age (ka)
B.
U1343
Laminations
U1345
Laminations
Insolation (65°N)
[W/m2]
520
510
500
490
480
470
460
3
3.5
4
4.5
5
MIS 11

Figure 3.

Figure 3A. Age model plotted by depth. Blue plots depict data from Site U1343, red 2 plots are from U1345. Magnetic susceptibility and benthic foraminiferal $\delta^{18}O$ are plotted 3 by depth for each Site in the top half of the figure. The grey line joining the magnetic 4 susceptibility plots indicates the tie point that was added in this study. Inverted triangles 5 indicate locations of tie points (red: U1345, blue: U1343, grey: magnetic susceptibility) 6 between Bering Sea $\delta^{18}O$ (Cook et al., 2016; Asahi et al., 2016) and the global marine 7 stack (Lisiecki and Raymo, 2005), which is plotted in grey. **B**: Age model plotted by age. 8 Magnetic susceptibility and $\delta^{18}O$ are shown with the global marine $\delta^{18}O$ stack (grey) and 9 insolation at 65° N (orange). Green bars indicate laminated intervals in U1343 and U1345.

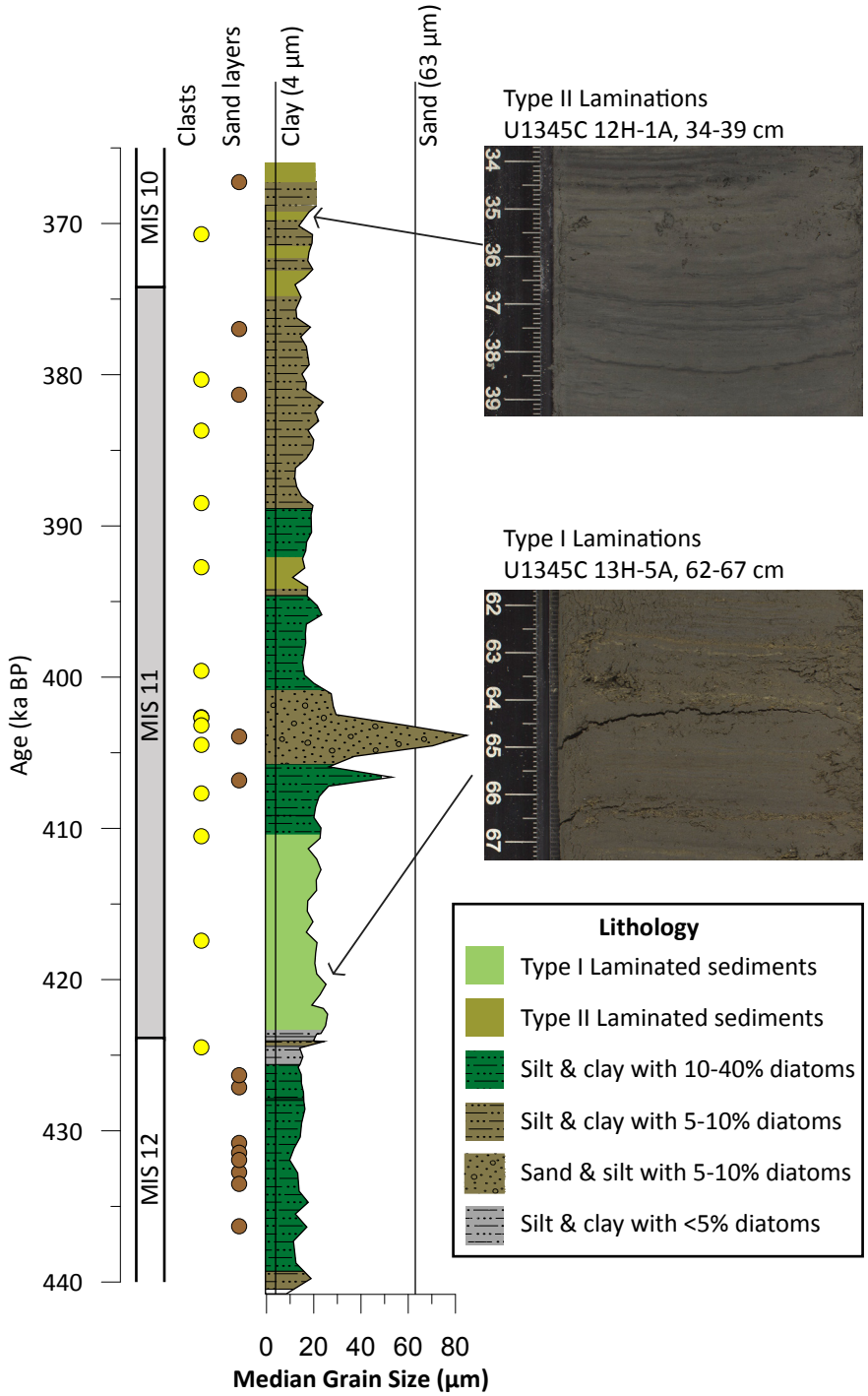

Figure 4. Lithostratigraphic column for U1345A. Marine Isotope Stage 11 is depicted as a grey bar. Ice rafted debris (yellow dots) and sand layers (maroon dots) are a compilation of these features in all four holes at U1345. The width of the lithologic column varies according to median grain size. Vertical lines indicate the cut off for clay and sand sized particles. Silt lies between the two lines. Colors depict varying amounts of diatoms relative to terrigenous grains in the sediment. Type I Laminations are depicted as pale green bars and Type II laminations are depicted as olive green bars. An example of each of the lamination types is shown in the images to the right.

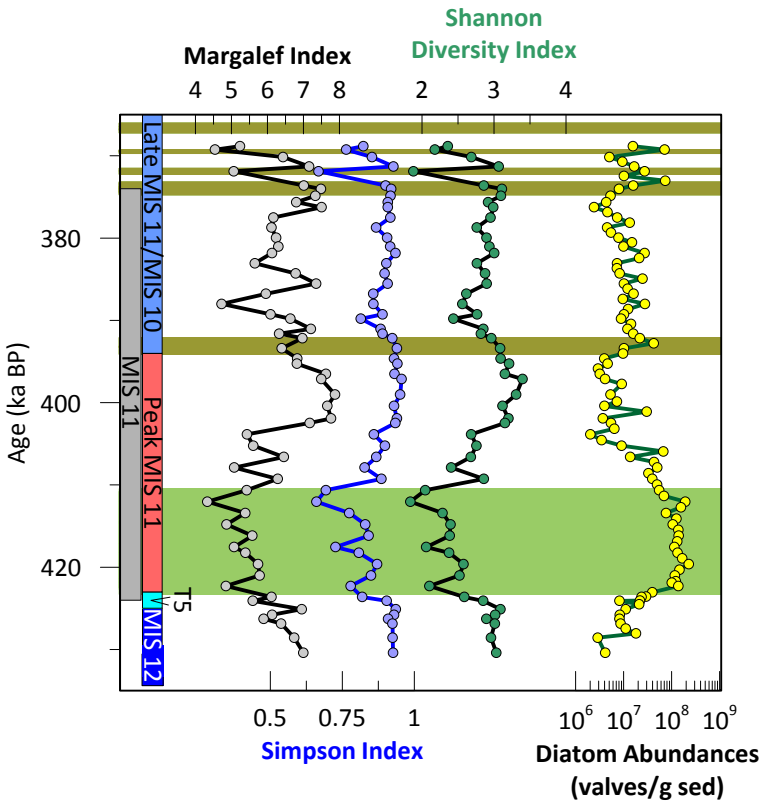

Figure 5. The Margalef, Simpson, and Shannon diversity indices plotted with diatom abundances. Type I Laminations are depicted as pale green bars and Type II laminations are depicted as olive green bars. Colored vertical bars refer to the zones mentioned in the text.

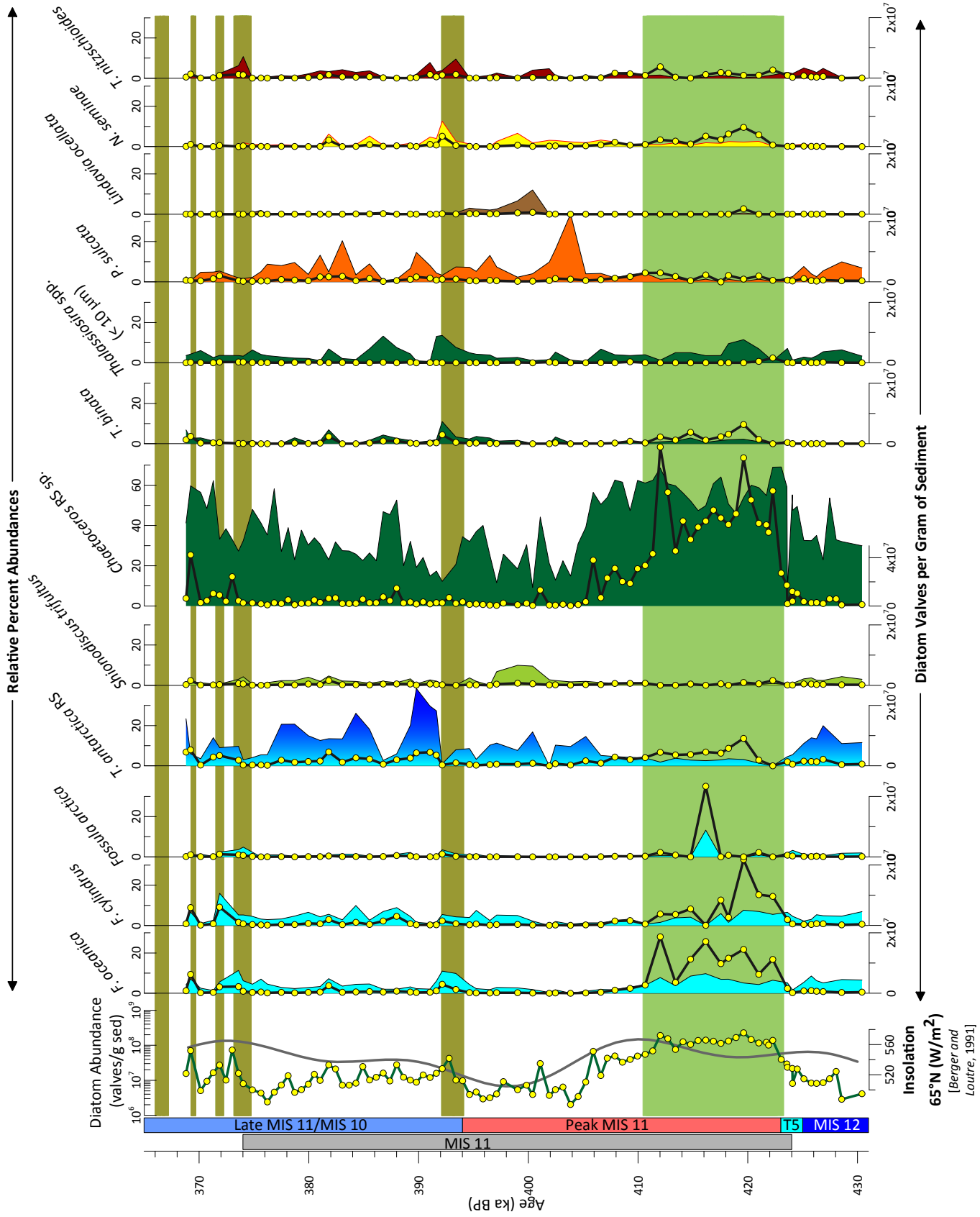
Relative Percent Abundances
Diatom Valves per Gram of Sediment
T. nitzschioides
N. seminae
Lindavia ocellata
P. suiceta
Thalassiosira spp. (< 10 µm)
T. binata
Chaetoceros RS sp.
Shionodiscus trifultus
T. antarctica RS
Fossula arctica
F. cylindrus
F. oceanica
Diatom Abundance (valves/g sed)
Insolation 65°N (W/m2) [Berger and Loutre, 1991]
Late MIS 11/MIS 10
Peak MIS 11
T5
MIS 12
MIS 11
Age (ka BP)

Figure 6.

Figure 6. Absolute and relative percent abundances of all diatoms that occur in 15 abundances greater than 10% of any assemblage. Colored vertical bars refer to the zones 16 mentioned in the text. Line plots depict absolute abundance and area plots depict relative 17 percent abundance. Species are color coded according to the niche that they are grouped 18 into: marginal ice zone (light blue), both ice types (dark blue to light blue), dicothermal 19 (light green), high productivity (green), neritic (orange), freshwater (brown), North 20 Pacific (yellow), and warm water (red). Insolation 65° N (light grey line) is also shown. 21 Type I Laminations are depicted as pale green bars and Type II laminations are depicted 22 as olive green bars.

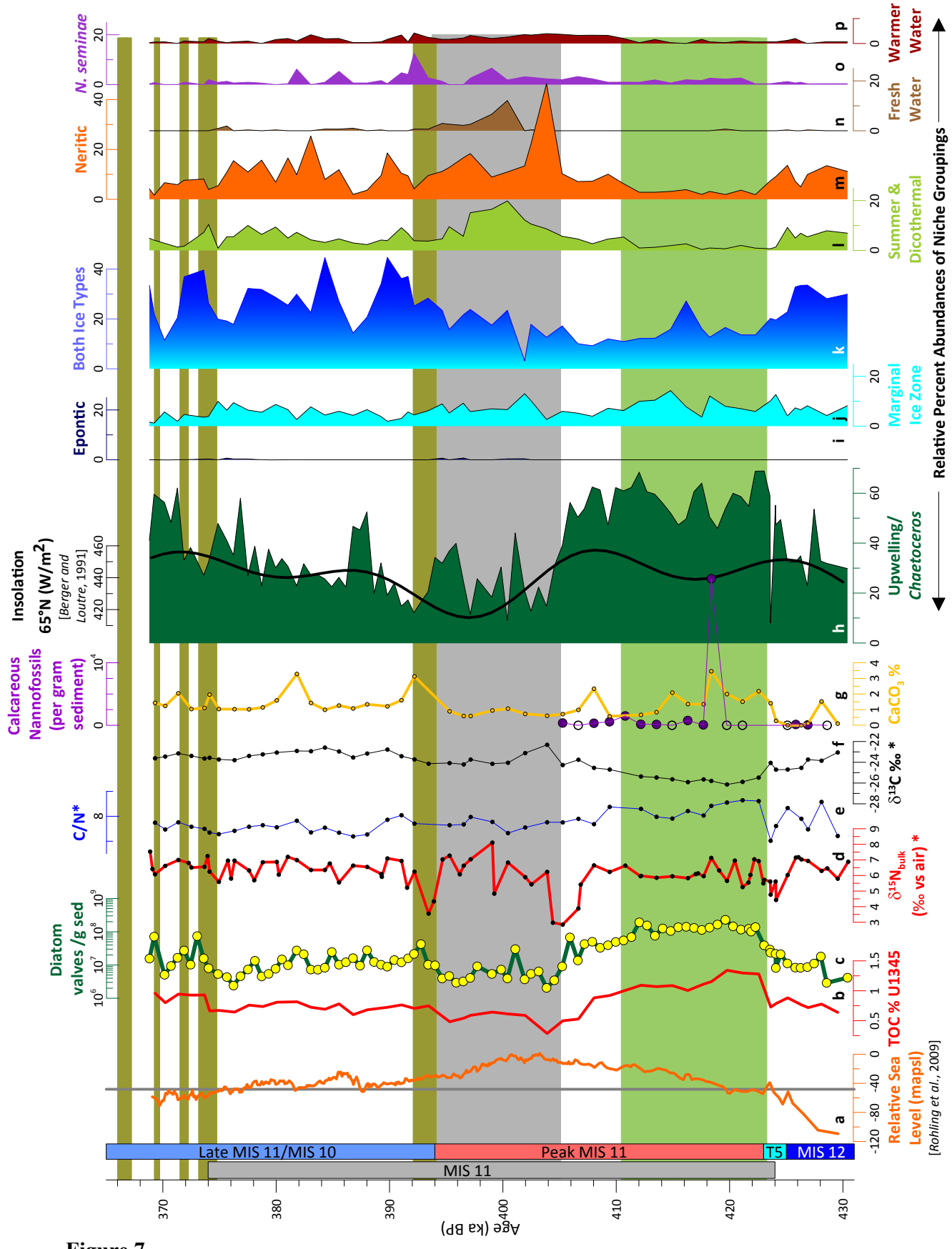
Insolation 65°N (W/m2) [Berger and Loutre, 1991]
Calcareous Nannofossils (per gram sediment)
Diatom valves /g sed
C/N*
Relative Sea Level (mapsl) [Rohling et al., 2009]
TOC % U1345
δ15Nbulk (‰ vs air) *
δ13C ‰ *
CaCO3 %
Upwelling/ Chaetoceros
Epontic
Both Ice Types
Marginal Ice Zone
Neritic
N. seminae
Summer & Dicothermal
Fresh Water
Warmer Water
Relative Percent Abundances of Niche Groupings
Late MIS 11/MIS 10
Peak MIS 11
T5
MIS 12
MIS 11
Age (ka BP)

Figure 7.

Figure 7. Summary of geochemistry and biological proxies. The grey vertical bar depicts the duration of MIS 11 and colored vertical bars refer to the zones mentioned in the text. **A.** Global eustatic sea level (orange) is plotted for reference (Rohling et al., 2010). The sill depth of Bering Straight (-50 m apsl) is shown as a vertical grey line. Total organic carbon (**B.** red) is plotted with the total diatom abundance (**C.** green line, yellow dots). Geochemical data is plotted as $\delta^{15}N$ (**D.** red), C/N (**E.** blue), $\delta^{13}C$ (**F.** black), and % $CaCO_3$ (**G.** yellow). Biological proxies include absolute abundance of calcareous nannofossils (**G.** purple). Open circles indicate barren samples; closed circles indicate samples that had calcareous nannofossils present. Relative percent abundances of diatoms are grouped by environmental niche. *Chaetoceros* RS are green (**H.),** epontic species are navy blue (**I.**), marginal ice zone species are light blue (**J.**), species that fall under both ice categories are shaded with a gradational blue (**K.**), summer and dicothermal species are light green (**L.**), neritic species are orange (**M.**), fresh water species are brown (**N.**), *N. seminae* is purple (**O.**), and warmer water species are maroon (**P.**). Insolation at 65° N (black) is overlain on *Chaetoceros* RS relative percent abundances. Type I Laminations are depicted as pale green bars and Type II laminations are depicted as olive green bars. A grey bar indicates the Beringian glacial advance.

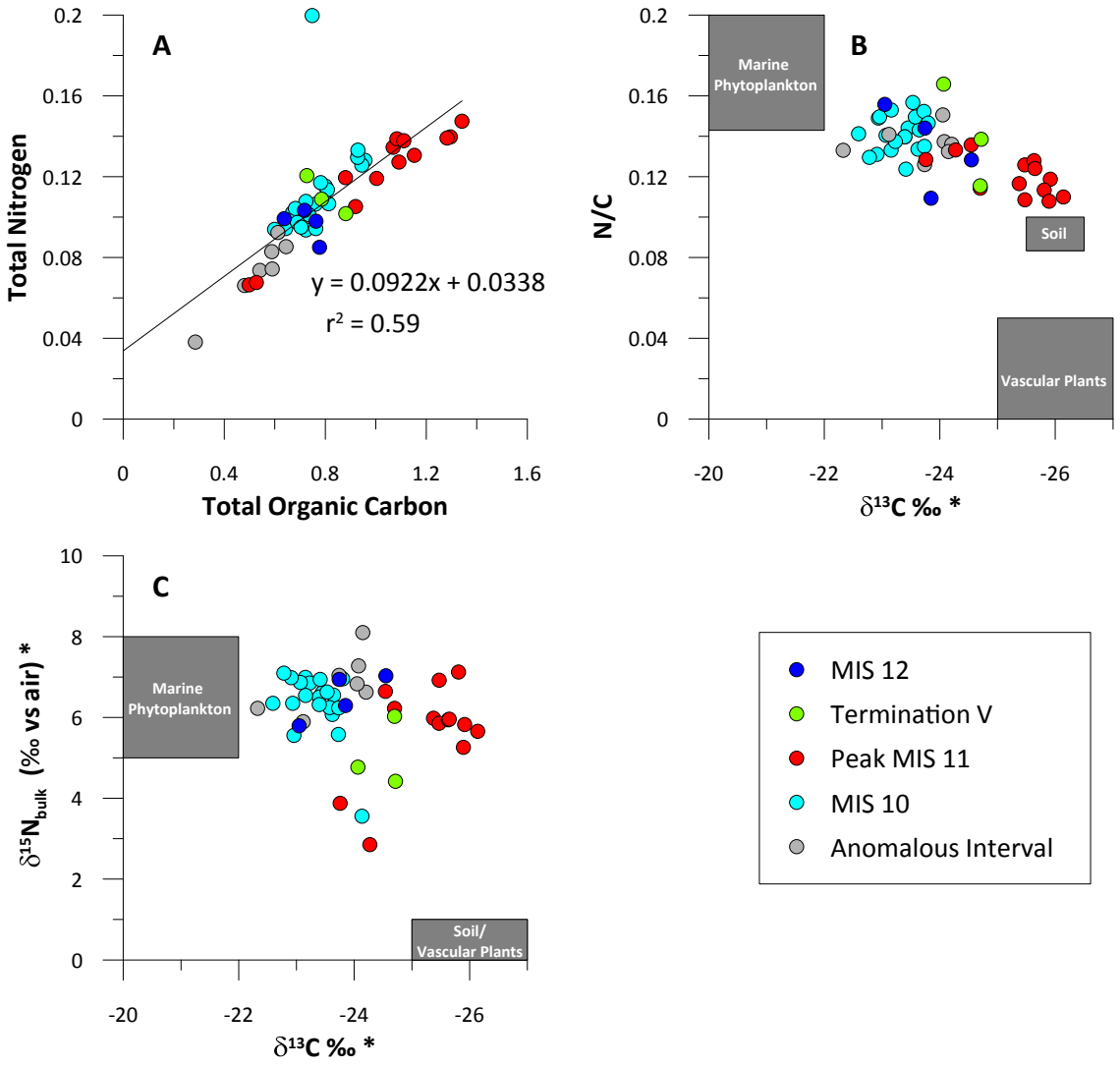

Figure 8. Crossplots of **A.** total nitrogen vs. total organic carbon, **B.** N/C_{rg} vs. $\delta^{13}C$, and **C**. $\delta^{15}N$ vs. $\delta^{13}C$. For each panel, the range of composition of each organic matter source is plotted in a grey box: marine phytoplankton (C/N: 5-7 (Redfield, 1963; Meyers, 1994); $\delta^{13}C$: -19‰ to -22‰ (Schubert and Calvert, 2001); $\delta^{15}N$: 5‰ to 8‰ (Walinsky et al., 2009)); Soil (C/N: 10-12, $\delta^{13}C$: -25.5‰ to -26.5‰, $\delta^{15}N$: 0‰ to 1‰ (Walinsky et al., 2009)); C3 vascular plants (C/N: > 20 (Redfield, 1963; Meyers, 1994); $\delta^{13}C$: -25‰ to -27‰ (Schubert and Calvert, 2001); $\delta^{15}N$: 0‰ to 1‰ (Walinsky et al., 2009)).

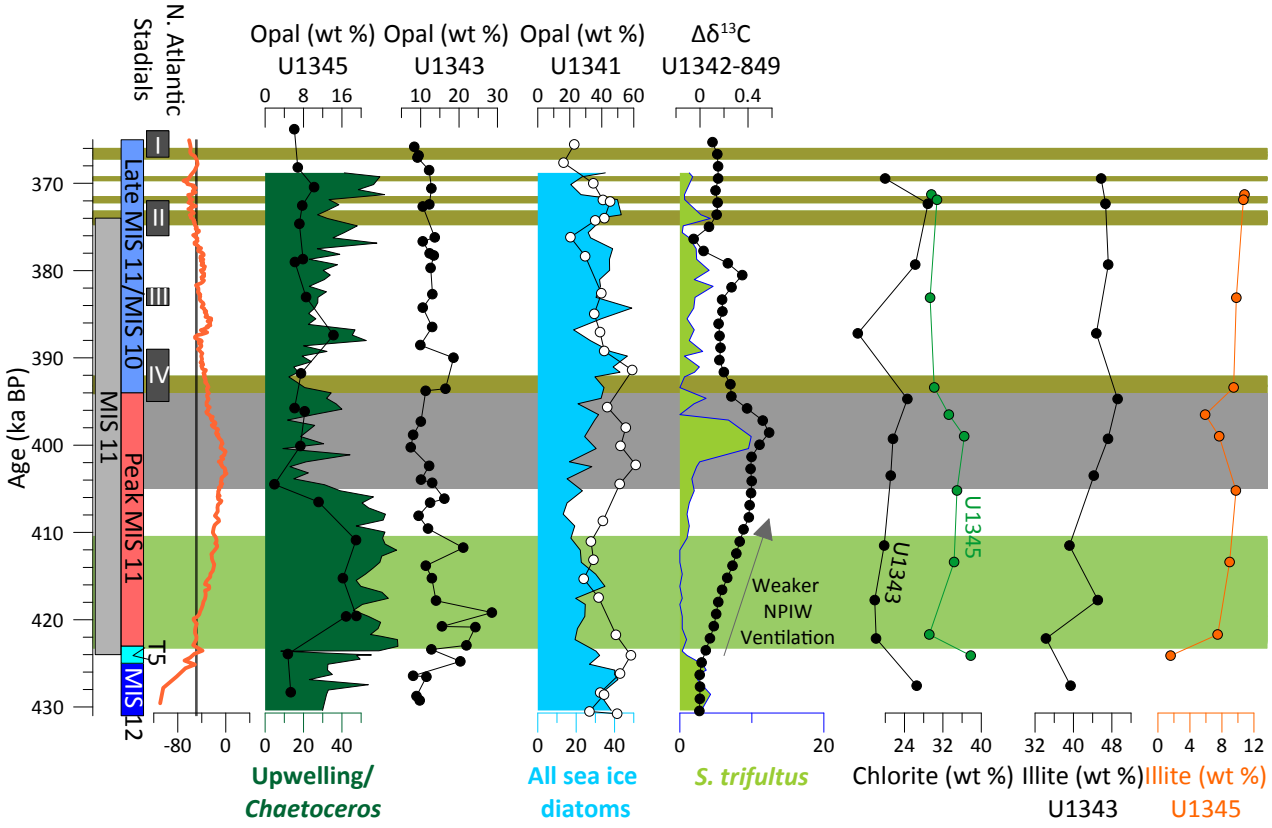

Figure 9. Comparison of Site U1345 with other Bering Sea (U1340, U1341, U1343) and global sites. The grey vertical bar depicts the duration of MIS 11, colored vertical bars refer to the zones mentioned in the text, and dark grey bars show the timing of North Atlantic stadials (I-IV) (Voelker et al., 2010). Global eustatic sea level (orange) is plotted for reference (Rohling et al., 2010). The sill depth of Bering Straight (-50 m apsl) is shown as a vertical grey line. Weight % opal from Sites U1345, U1343, and U1341 (Kanematsu et al., 2013) is plotted with *Chaetoceros* RS relative percent abundances, and relative percent abundances of all sea ice diatoms. The difference in benthic foraminiferal $\delta^{13}C$ between the Bowers Ridge (U1342) and the North Pacific (ODP 849), a proxy for North Pacific Intermediate Water ventilation, is plotted with relative percent abundances of *Shionodiscus trifultus,* an indicator of highly stratified water. Note that ventilation increases to the left. The weight percent of the clay minerals, chlorite and illite are plotted for Sites U1343 (Kim et al., 2015) and U1345 (this study). Type I Laminations are depicted as pale green bars and Type II laminations are depicted as olive green bars. A grey bar indicates the "anomalous interval."

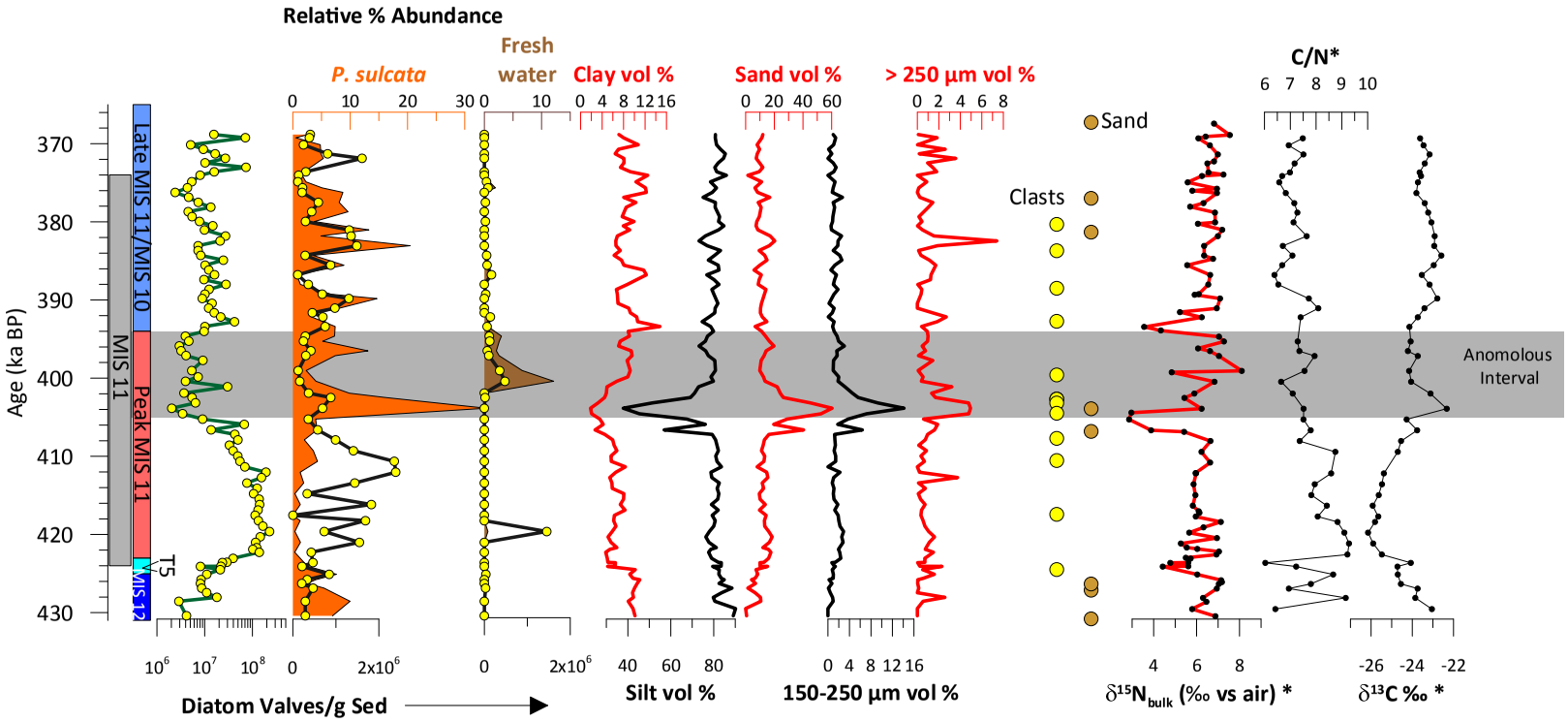

Figure 10. Proxy indicators of shelf to basin transport. The grey vertical bar depicts the duration of MIS 11, colored vertical bars refer to the zones mentioned in the text. Total diatom absolute abundances are plotted next to absolute (line plots) and relative percent abundance of P. sulcata (orange area plot) and fresh water species (brown area plot). High-resolution grain size includes % clay, sand, and greater than 250 µm (red lines) and % silt and 150-250 µm (black lines). Yellow circles indicate isolated clasts (IRD), maroon circles indicate sand layers for all holes at U1345. Geochemical data is plotted as δ15N (red), C/N (black), and δ13C (black). The grey bar spans 405-394 ka, the so-called, "anomalous interval."